Pergamon

Geochimica et Cosmochimica Acta, Vol. 68, No. 5, pp. 1135–1157, 2004

0016-7037/04 $30.00 + .00

doi:10.1016/j.gca.2003.07.014

Petrographic and oxygen-isotopic study of refractory forsterites from R-chondrite Dar al Gani 013 (R3.5-6), unequilibrated ordinary and carbonaceous chondrites

ANDREAS PACK,[1,*,†] HISAYOSHI YURIMOTO,[2] and HERBERT PALME[1]

[1]Institut für Mineralogie und Geochemie, Universität Köln, Zülpicher Straße 49b, D-50649 Köln, Germany
[2]Tokyo Institute of Technology, Department of Earth and Planetary Science, Meguro, Tokyo, Japan

(*Received October* 31, 2002; *accepted in revised form July* 23, 2003)

Abstract—We have conducted petrographic, chemical and in-situ oxygen isotopic studies of refractory forsterites from unequilibrated ordinary and carbonaceous chondrites as well as an unequilibrated R-chondrite. Refractory forsterites occur in all types of unequilibrated chondrites and all have very similar chemical composition with low FeO and high refractory lithophile element (RLE) contents. Refractory forsterites are typically enriched in ^{16}O relative to 'normal' olivine independent of the bulk O-isotope ratios of the parent meteorites. Analyses of refractory forsterites spread along a $\Delta^{17}O$ mixing line with $\Delta^{17}O$ ranging from +2 to −10‰. Due to similarities in oxygen isotopes and chemical compositions, we conclude that refractory forsterites of various types of chondrites come from a single common reservoir. Implications of this hypothesis for the chemical and O-isotope evolution of silicates in the early solar nebular are discussed. *Copyright © 2004 Elsevier Ltd*

1. INTRODUCTION

1.1. Formation Models of Refractory Forsterite

The first major silicate phase to condense from a gas of solar composition is FeO-poor olivine (Larimer and Anders, 1967; Grossman, 1972; Ebel, 2000; Ebel and Grossman, 2000). Such forsterites should have ~0.2 mol% fayalite and MnO and NiO contents in the ppm range (Palme and Fegley, 1990).

Reid et al. (1970) and Fuchs et al. (1973) were the first to describe isolated FeO-poor, refractory forsterite grains from carbonaceous chondrites (e.g., Fig. 1A). Steele (1985, 1986a, 1995) identified refractory forsterite grains by cathdoluminescence (CL) microscopy (Fig. 1B) and related blue luminescence to high contents of refractory lithophile elements (RLE) accompanied by low contents of FeO (<1–2 wt%). Refractory forsterites are also extremely poor in NiO and MnO, in addition to being rich in RLEs including CaO (0.4–0.8 wt%), Al_2O_3 (0.2–0.3 wt%), TiO_2 (≤0.15 wt%) and REEs (Klerner et al., 2000; Weinbruch et al., 2000; Klerner 2001; Pack et al., 2003). Refractory forsterite grains range in size from <10 μm up to ≈500 μm and occur as isolated mineral grains in chondrite matrices (see Fig. 1A) as well as within chondrules. Concentrations of CaO and other RLEs typically decrease towards the rims of refractory forsterites, whereas FeO and MnO increase (Fig. 1C).

Two theories for the origin of refractory forsterite are proposed. Reid et al. (1970) and Fuchs et al. (1973) concluded that these forsterite grains represent condensates from the solar nebula (Grossman and Olsen, 1974; Olsen and Grossman, 1978; Steele, 1986b, 1989; Weinbruch et al., 1993, 2000; Klerner, 2001) and that melt inclusions in them are also direct condensates (Fuchs et al., 1973; Yoneda and Grossman, 1995). Melt condensates may form when the equilibrium condensation temperatures of mineral assemblages exceed their solidus temperatures. In such a case, melts are in equilibrium with the gas phase, i.e., form stable condensates. Melt condensates differ from chondrule melts, which formed by heating and melting of a solid precursor material. Other authors (McSween, 1977; Richardson and McSween, 1978; Roedder, 1981; Desnoyers, 1980; Jones, 1992, 1996; Leshin et al., 1997; Jones et al., 2000a) suggested formation of refractory forsterites by crystallization within FeO-poor and RLE-rich type-I chondrules. Preferential fragmentation of chondrules along crystal faces released euhedral forsterite grains, some of which reentered chondrules (xenocrysts in chondrules) and others accreted together with fine-grained matrix material (isolated grains). They suggest that melt inclusions represent entrapped melt from the parental chondrule instead of being melt condensates. Jones (1992) compared isolated refractory forsterites with those from within chondrules. She concluded, based on similarities in major and minor element signatures, that isolated forsterites grains were originally derived from type-I (FeO-poor) chondrules.

New experimental data on the equilibrium Ca-partitioning between forsterite and melt (Libourel, 1999) unambiguously demonstrate that high concentrations of CaO (0.6–0.8 wt%) in refractory forsterite require a melt containing 20–22 wt% CaO. McSween (1977) suggested that high CaO concentrations could be the result of disequilibrium partitioning between melt and rapidly growing olivine. Kennedy et al. (1993), Pack et al. (2002a) and Pack and Palme (2003), however, demonstrated that partitioning of Ca between forsterite and silicate melts is independent of the cooling rate (1.5 to >2000°C/h) at CaO-contents ranging from <5 to ≈25 wt%. Hence, if refractory forsterites crystallized from a melt, it must have been unusually rich in RLEs.

* Author to whom correspondence should be addressed (apack@crpg.cnrs-nancy.fr).
† *Present address:* CRPG/CNRS Centre de Recherches Pétrographiques et Géochimiques, 15 rue Notre Dame des Pauvres, 54501 Vandoeuvre-lès-Nancy, France.

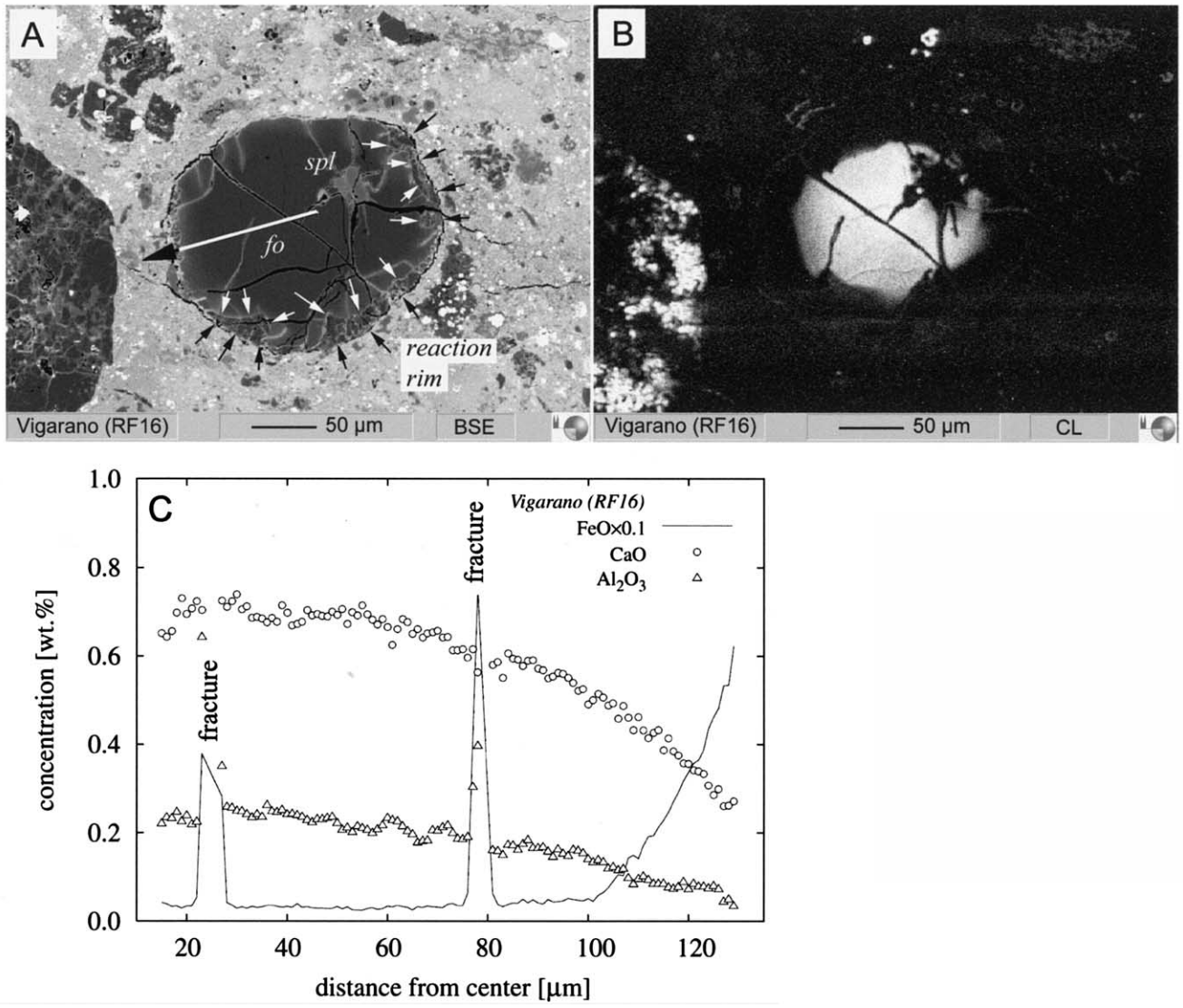

Fig. 1. Backscattered electron (A) and CL-image (B) of an isolated refractory forsterite grain from Vigarano (CV3). A spinel grain is enclosed in the forsterite. Veinlets, cross cutting the forsterite, as well as the outer rim are too FeO-rich (>~2 wt%) to exhibit CL emission. The rim of the forsterite is partially replaced by pyroxene-rich materials (arrows). C) Chemical profile (EPMA) from center to the rim of the refractory forsterite. Note the smooth decrease in CaO and Al_2O_3 and the increase in FeO towards the rim of the grain.

1.2. Oxygen Isotope Ratios of Refractory Forsterites

It was suggested by Steele (1986b) that by analyzing oxygen isotope ratios in refractory forsterites it would be possible to determine whether refractory forsterites are ^{16}O-rich condensates or whether they mirror the oxygen isotope ratios of more isotopically normal chondrule hosts. Since then, ^{16}O-enriched ($\delta^{17}O \geq -15‰$, $\delta^{18}O \geq -10‰$) refractory forsterite grains have been reported from carbonaceous (Hervig and Steele, 1992; Weinbruch et al., 1993; Leshin et al., 1997, 2000) and ordinary chondrites (Saxton et al., 1998; Sears et al., 1998; Ruzicka et al., 2000). Recent determinations of oxygen isotope ratios of bulk chondrules from carbonaceous chondrites (Jones et al., 2000b) and chondrule components from Al-rich ordinary chondrites (Russell et al., 2000), provide evidence for the existence of ^{16}O-rich chondrule melts outside the 'traditional' chondrule fields defined by Clayton et al. (1983, 1991). Enrichment in ^{16}O of refractory forsterites, therefore, cannot be taken as evidence for a condensation origin.

Refractory, ^{16}O-rich forsterite apparently is a widespread component in both carbonaceous (CCs) and unequilibrated ordinary chondrites (UOCs), although bulk oxygen isotope data of carbonaceous chondrites CCs and UOCs are very different. Either these forsterites formed at a single nebular location by condensation from a gas or by crystallization from RLE-rich melts and were later transported to their accretion locations or they formed at different locations with identical initial evolution.

We have begun a comprehensive study of forsteritic olivine grains in all types of chondritic meteorites with the exception of

Table 1. Abundances of luminescent refractory forsterites (in vol%) from different types of chondrites. Name, group and petrologic type of the samples are indicated (UOC: unequilibrated ordinary chondrite; RC: Rumurutiite; CC: carbonaceous chondrite; n.d.: not determined).

Sample	Group	Type	Section	Area (mm^2)	Vol%
Semarkona	UOC	LL3.0	UNM	154	0.08
Bishunpur	UOC	LL3.1	Bish	36	0.07
Chainpur	UOC	LL3.4	Cha	128	0.14
Chainpur	UOC	LL3.4	Cha1	177	0.28
Dar al Gani 369	UOC	L(H)3	DaG369	415	0.007
Dar al Gani 378	UOC	H(L)3	DaG378	290	0.012
Dar al Gani 327	UOC	H3	DaG327	284	0.005
Dar al Gani 405	UOC	H3	DaG405	128	0.08
Dar al Gani 013	RC	R3.5-6	PL96217	182	0.02
Dar al Gani 013	RC	R3.5-6	PL96218	163	0.028
Dar al Gani 013	RC	R3.5-6	PL95141	706	0.003
Murchison	CC	CM2	Mur-RE	56	0.35
Renazzo	CC	CR2	1355	156	0.13
Leoville	CC	CV3	RE-S	13	0.24
Kaba	CC	CV3	Köln	28	0.005
Allende	CC	CV3	All-3	158	0.04
Vigarano	CC	CV3	Vig1	n.d.	n.d.
Dar al Gani 430	CC	C3 (ungrouped)	DaG430	150	0.009
Hammadah al Hamra 180	CC	C3 (ungrouped)	HaH180	144	0.003

enstatite chondrites. In a first step we have systematically searched for luminescent forsterites in sections of different chondritic meteorites.

The purpose of this investigation is two-fold: (1) To determine if the forsterite grains represent a single population that is common to OCs, RCs and CCs and thus provides a link between them, and (2) to better constrain the formation conditions of forsteritic olivine grains, either by condensation from a nebular gas or by crystallization from chondrule melts.

2. SAMPLES AND ANALYTICAL TECHNIQUES

Petrographic studies were done on 18 polished thin-sections of 16 different unequilibrated chondrites (Table 1). Refractory forsterites were identified by cathodoluminescence (CL) microscopy using a black and white CL-detection unit attached to a JEOL 8900RL electron microprobe. The volumetric abundance of luminescent forsterite (Table 1) was determined by point counting and calculated using the relation (Schneiderhöhn and Ramdohr, 1934):

$$C_{lum.fo}^{\text{section}}\,[vol\%] = 100 \times \frac{A_{lum.fo}[mm^2]}{A_{\text{section}}[mm^2]}\,[vol\%].$$

$C_{lum.fo}^{\text{section}}$ is the volume percentage of luminescent forsterite, $A_{lum.fo}$ the area of luminescent forsterite in the section and $A_{section}$ the total area of the section. Only the luminescent areas of olivine grains were considered. The JEOL probe was also used for chemical micro-analyses (Table 2) as well as backscattered electron (BSE) imaging. Element analyses were performed using wavelength dispersive spectrometers at an accelerating voltage of 15 kV and a beam current of 20 nA. A set of natural and synthetic silicate and oxide standards was used for calibration procedures. Detection limits are in the ranges of $\leq$0.05 wt%, depending on the element and the measurement conditions.

High spatial resolution oxygen isotope ratios (Table 3) were measured using the Tokyo Institute of Technology (TiTech) Cameca 1270 SIMS with a primary Cs^+ beam of $\approx$5 μm diameter and a spot size of $<$10 μm. An electron flood gun was used to compensate electrostatic charging of the carbon-coated sample surface. The mass resolving power was adjusted to 6000 to resolve the interference of ^{16}OH on the ^{17}O-peak. A terrestrial spinel and an olivine standard (San Carlos) were used for calibration and correction of internal mass fractionation. The instrumental mass fractionation (IMF) between the olivine and the spinel was determined to be $\delta^{17}O_{ol} - \delta^{17}O_{spl} = -3.6 \pm 1‰$ and $\delta^{18}O_{ol} - \delta^{18}O_{spl} = -6.9 \pm 1‰$. The measured data were corrected for IMF depending on the analyzed individual sample (ol, spl) and which standard was used. Preliminary data were presented in part by Pack et al. (2002b, not corrected for IMF). Since only olivine and spinel was used for calibration, analyses of mesostasis glass (see Pack et al., 2002b) were removed from the data set due to unknown IMF effects. After ion probe analyses, the position of the ion probe spots were checked by optical microscopy and scanning electron microscopy (SEM) to ensure that the spots were located on clean mineral surfaces.

The error ellipses that are displayed in the 3 − O-isotope diagrams indicate the estimated accuracy of 68% confidence. Enrichments in ^{16}O are expressed as the permil deviation from the terrestrial mass dependent fractionation line with $\Delta^{17}O = \delta^{17}O - 0.524 \times \delta^{18}O$. The error intrinsic to the $\Delta^{17}O$ value is $\pm$ 2.7‰ (1σ).

3. RESULTS

3.1. Abundance of Refractory Forsterite

The results of the point counting study are given in Table 1. The abundance of luminescent refractory forsterite varies between $<$0.01 and 0.35 vol%. The carbonaceous chondrite Murchison (CM2) contains the highest concentration of refractory forsterites (0.35 vol%), followed by ordinary chondrite Chainpur (LL3.4, 0.28 vol%) and carbonaceous chondrite Leoville (CV3, 0.24 vol%).

Table 2. EPMA analyses of refractory forsterites and associated mineral phases from various unequilibrated chondrites (data are reported in wt.%). The mineral formulae were calculated based on the number of oxygens per formula unit.

Sample	Dar al Gani 013						Chainpur						
Location	RF08			RF10		Matrix	Cha/C1				Cha1/C1		
Phase	*fo*	*fo*	*fa-rim*	*fo*	*fa-rim*	*fa*	*fo*	*fa*	*slp*	*meso*	*fo*	*fo*[a]	*meso*
SiO_2	43.72	43.66	42.05	43.65	43.05	34.98	42.84	42.58	0.19	50.23	42.24	42.77	52.91
TiO_2	0.07	0.08	<0.05	0.07	<0.05	<0.05	0.08	<0.05	0.27	0.24	0.06	<0.05	0.61
Al_2O_3	0.26	0.62	0.06	0.44	0.04	0.03	0.28	0.04	69.16	27.87	0.19	0.02	20.49
Cr_2O_3	0.10	0.08	0.10	0.08	0.09	0.15	0.09	0.04	0.56	0.06	0.13	0.07	0.45
FeO	0.36	0.40	11.19	0.36	5.41	34.04	0.40	4.27	4.65	1.57	0.51	0.69	0.38
MnO	0.02	0.01	0.13	<0.01	0.05	0.39	0.02	0.08	0.04	0.01	<0.01	0.03	0.19
MgO	55.26	54.99	47.12	54.89	52.62	30.50	56.94	53.38	25.17	2.36	56.13	56.71	9.42
CaO	0.68	0.57	0.13	0.66	0.25	0.21	0.69	0.29	0.01	13.95	0.52	0.11	14.15
Na_2O	<0.03	<0.03	<0.03	<0.03	<0.03	<0.03	<0.03	<0.03	<0.03	3.23	<0.03	<0.03	2.31
K_2O	<0.02	<0.02	<0.02	<0.02	<0.02	<0.02	<0.02	0.02	<0.02	0.28	<0.02	<0.02	<0.02
Σ [oxides]	100.47	100.40	100.77	100.14	101.50	100.31	101.34	100.71	100.03	99.79	99.79	100.40	100.92
O [p.f.]	4	4	4	4	4	4	4	4	4	—	4	4	—
Si	1.020	1.018	1.024	1.021	1.015	0.966	0.994	1.009	0.005	—	0.996	1.001	—
Ti	0.001	0.001	—	0.001	—	—	0.001	—	0.005	—	0.001	—	—
Al	0.007	0.017	0.002	0.012	0.001	0.001	0.008	0.001	1.974	—	0.005	0.001	—
Cr	0.002	0.001	0.002	0.001	0.002	0.003	0.002	0.001	0.011	—	0.002	0.001	—
Fe	0.007	0.008	0.228	0.007	0.107	0.786	0.008	0.085	0.094	—	0.010	0.014	—
Mn	0.000	0.000	0.003	—	0.001	0.009	0.000	0.002	0.001	—	—	0.000	—
Mg	1.921	1.911	1.710	1.913	1.849	1.256	1.969	1.885	0.908	—	1.972	1.978	—
Ca	0.017	0.014	0.003	0.016	0.006	0.006	0.017	0.007	0.000	—	0.013	0.003	—
Na	—	—	—	—	—	—	—	—	—	—	—	—	—
K	—	—	—	—	—	—	—	—	—	—	—	—	—
Σ [c.p.f.]	2.975	2.971	2.972	2.971	2.981	3.028	3.000	2.989	2.998	—	2.999	2.997	—
fa [mol%]	0.4	0.4	11.4	0.4	5.3	39.3	0.4	4.2	—	—	0.5	0.7	—

[a] Nonluminous forsteritic olivine.
[b] Average of 12 analyses.
[c] Average of three analyses.

3.2. Mineral Chemistry

In Table 2 we have compiled results of the microprobe analyses of refractory forsterite grains and related phases in various types of unequilibrated chondrites. Refractory forsterites are FeO-poor with a lower limit of 0.2 wt% FeO. Concentrations of CaO vary between 0.4 and 0.7 wt%. Al_2O_3 is typically 0.2–0.3 wt% in refractory forsterites. Concentrations of Cr_2O_3 vary around 1000 ppm (500–2000 ppm). Concentrations of MnO are low in the refractory forsterites, but increase with increasing FeO content of the olivines. TiO_2 contents vary in a range between <0.05 and 0.1 wt%. The fayalitic rims and fayalitic olivines are enriched in MnO. The enrichment in FeO and MnO is accompanied by a depletion in CaO and Al_2O_3 as compared to the refractory cores (see Fig. 1C).

Some of the refractory forsterites contain spinel inclusions. The spinel in refractory forsterite Cha/C1 (Chainpur, Figs. 2A,B) is a low-Cr Mg, Al-spinel with 9.4 mol% hercynite and 0.55 mol% magnesiochromite ($MgCr_2O_4$). The spinel inclusion in forsterite grain Mur/RF07 (Fig. 10E) from Murchison contains 2.5 mol% hercynite and 8.7 mol% magnesiochromite. The spinel inclusion in RF16 from Vigarano (Fig. 1A) contains 26.8 mol% hercynite and 0.5 mol% magnesiochromite.

3.3. Petrography and Oxygen Isotope Ratios

In the following section, the petrography and O-isotope compositions of refractory forsterites are discussed separately for each individual chondrite. The oxygen isotope ratios are plotted in $\delta^{17}O$ vs. $\delta^{18}O$ diagrams. For reference, the terrestrial fractionation line (TFL: $\delta^{17}O = 0.524 \times \delta^{18}O$) is displayed, along with postulated primordial ^{16}O exchange lines, the carbonaceous chondrite anhydrous mineral mixing line (CCAM: $\delta^{17}O = 0.94 \times \delta^{18}O - 4.06‰$; Clayton et al., 1977), and the Young and Russell (1998) line (Y&R: $\delta^{17}O = \delta^{18}O - 1‰$).

In Table 3 the results of the oxygen isotope measurements are reported, relative to the V-SMOW oxygen isotope standard.

3.3.1. Chainpur (LL3.4)

Chondrule Cha/C1 is a 650 μm large macroporphyritic, spinel-bearing chondrule. The chondrule hosts a single 300×600 μm large, partially corroded refractory forsterite grain (Figs. 2A,B). Several luminescent, presumably fragments of the large forsterite grain (Fig. 2B) are scattered in the fine grained calcic mesostasis. The forsterite exhibits homogenous bright CL-emission and is surrounded by a nonluminous rim, a few microns thick. Several 40–50 μm large, euhedral to subhedral spinel ($Mg_{0.91}Fe_{0.09}Al_{1.98}Cr_{0.01}O_4$) inclusions occur in the interior of the large olivine grain along with two melt inclusions. The melt inclusions may actually represent melt channels cross-cutting the forsterite in the third dimension, suggested by the absence of shrinkage bubbles. The opaque phase in chondrule Cha/C1 is troilite (FeS). The mesostasis is submicroscopically fine grained and composed of calcic pla-

Chainpur		Dar al Gani 378			Dar al Gani 369						Allende	
Cha/Iso-1	Cha1/Iso-1	RF03	RF05	BOC	RF02				RF05	RF06	RF03	
fo	*fo*	*fo*	*fo*	*BO*	*fo*	*fa*	*incl*	*meso*[b]	*fo*	*fo*	*fo*	*fa*
41.88	41.12	41.53	41.75	36.38	42.63	37.66	40.20	63.95	42.60	41.97	42.80	38.21
<0.05	0.05	0.06	<0.05	<0.05	0.05	<0.05	0.74	0.98	<0.05	0.05	0.05	<0.05
0.13	0.31	0.27	0.23	0.03	0.29	0.04	29.46	20.87	0.18	0.28	0.23	0.09
0.14	0.10	0.12	0.13	0.13	0.05	<0.04	0.28	0.58	0.13	0.06	0.07	0.27
0.94	0.57	0.74	1.77	29.97	0.38	23.15	0.67	1.27	0.47	0.31	0.49	26.71
0.02	0.01	0.01	<0.01	0.61	0.02	0.20	0.04	0.03	0.01	0.01	0.02	0.15
56.77	56.76	56.73	56.13	32.42	56.76	39.68	2.24	0.06	56.47	56.48	56.28	35.82
0.41	0.58	0.48	0.49	0.05	0.56	0.19	3.40	0.03	0.41	0.67	0.67	0.11
<0.03	<0.03	<0.03	<0.03	<0.03	<0.03	<0.03	20.62	10.46	<0.03	<0.03	<0.03	<0.03
0.02	<0.02	<0.02	<0.02	0.02	<0.02	<0.02	2.61	2.40	<0.02	0.02	<0.02	0.02
100.30	99.49	99.93	100.49	99.61	100.74	100.91	100.24	100.64	100.28	99.84	100.60	101.37
4	4	4	4	4	4	4	—	—	4	4	4	4
0.985	0.975	0.980	0.984	0.991	0.995	0.976	—	—	0.998	0.989	1.000	1.000
—	0.001	0.001	—	—	0.001	—	—	—	—	0.001	0.001	—
0.003	0.009	0.007	0.006	0.001	0.008	0.001	—	—	0.005	0.008	0.006	0.003
0.003	0.002	0.002	0.002	0.003	0.001	0.000	—	—	0.002	0.001	0.001	0.006
0.019	0.011	0.015	0.035	0.682	0.007	0.502	—	—	0.009	0.006	0.010	0.584
0.000	0.000	0.000	—	0.014	0.000	0.004	—	—	0.000	0.000	0.000	0.003
1.991	2.006	1.996	1.971	1.316	1.974	1.533	—	—	1.972	1.983	1.960	1.397
0.010	0.015	0.012	0.012	0.000	0.014	0.005	—	—	0.010	0.017	0.017	0.003
—	—	—	—	—	—	—	—	—	—	—	—	—
0.001	—	—	—	—	—	—	—	—	—	0.000	—	0.001
3.012	3.018	3.013	3.010	3.007	3.000	3.022	—	—	2.996	3.006	2.995	2.996
0.9	0.6	0.7	1.7	34.1	0.4	25.1	—	—	0.5	0.3	0.5	29.2

gioclase and pyroxene. The large forsterite grain probably did not crystallize in situ in the chondrule as indicated by its embayed corroded surface. The large forsterite crystal is highly enriched in ^{16}O and plots slightly above the Y&R-line at $\delta^{18}O = -15‰$ (Fig. 3A). The spinel within the forsterite is even more enriched in ^{16}O and is in isotopic disequilibrium with its forsterite host, plotting on the Y&R line at $\delta^{18}O = -20‰$ (Fig. 3A).

Chondrule Cha1/C1 is an unusual porphyritic type-IA chondrule. It consists of porphyritic forsteritic olivine, embedded in a fine-grained calcic mesostasis (Figs. 2C,D). Olivine in the center of chondrule Cha1/C1 is nonluminous, whereas forsterite in the outer part of the chondrule shows weak CL-emission. Some olivine grains in the region between center and outer part exhibit unusual inverse CL-zoning, i.e., nonluminous forsterite is overgrown by luminescent forsterite (Fig. 2D). A chemical profile across an inversely zoned forsterite (Fig. 4) reveals CL emission to be correlated with enrichment in CaO which is accompanied by a parallel enrichment in Al_2O_3. Hence, high RLE, accompanied by low FeO contents are necessary for CL emission of forsterite (Steele, 1986a). Low FeO and RLE forsterite apparently does not exhibit CL.

The texture of chondrule Cha1/C1 is indicative of in situ crystallization of the luminescent forsterite. The increase in CaO from core to rim (Fig. 4) is compatible with closed system factional crystallization of these particular grains. The outermost decrease in CaO may be related to equilibration with the mesostasis at lower temperatures. Note that the width of the rim with decreasing CaO is very small (≈10 μm) compared to the profile shown in Figure 1C (≈60 μm). The luminescent forsterite from Cha1/C1 has a 'normal' oxygen isotope ratio with respect to OC chondrules ($\Delta^{17}O = +1.7‰$, Fig. 3B, Clayton et al., 1983; Gooding et al., 1983). The nonluminous chondrule olivine is not enriched in ^{16}O either, but exhibits significant mass fractionation along the TFL towards higher $\delta^{18}O$ by approximately +8‰ (Fig. 3B).

Isolated refractory forsterite grain Cha/Iso1 is ~50×80 μm in size and exhibits only a small area with CL emission (Fig. 2E). The luminescent as well as the nonluminous part of the grain are equally enriched in ^{16}O with $\delta^{17,18}O \approx -15‰$. Both, the luminescent forsterite and the nonluminous ferroan part plot on the CCAM to the 'right' of the Y&R-line (Fig. 3B).

Isolated refractory forsterite Cha1/Iso1 is irregularly shaped, ~200 μm in diameter (Fig. 2F). It comprises a refractory, luminescent core and a nonluminous rim. Cha1/Iso1 is not enriched in ^{16}O and plots near the bulk composition of Chainpur (Fig. 3B).

3.3.2. *Dar al Gani 369 (L(H)3)*

Chondrule DaG369/RF02 is a Na-, Al-rich chondrule consisting of porphyritic olivine and vitreous Na-, Al-rich mesostasis. The cores of the largest olivine grains ($fa_{0.4}$) show bright CL-emission with extinction of CL towards the more fayalitic rims (fa_{25}). The smaller, nonluminous grains are fayalite rich throughout (Fig. 5A). The mesostasis has a brownish tint in transmitted light and appears entirely amorphous between

Table 2. (Continued)

Allende					Renazzo	Murchison				Vigarano	
RF07		RF11	RF16	RF0S	RF06	RF05	RF07			RF16	
fo	*fa*	*fo*	*fo*	*fo*	*fo*	*fo*	*fo*[a]	*spl*	*cpx*[c]	*fo*	*spl*
42.92	39.69	43.01	42.67	40.55	42.51	42.38	40.81	0.15	46.71	43.03	0.16
0.08	0.07	0.09	<0.05	0.05	0.06	0.09	<0.05	0.35	2.11	0.08	0.16
0.54	0.66	0.26	0.26	0.21	0.20	0.28	0.31	62.44	10.97	0.22	66.69
0.11	0.23	0.07	0.05	0.09	0.14	0.06	0.20	8.97	0.34	0.11	0.51
0.30	15.15	0.29	0.20	0.47	0.53	0.35	2.01	1.21	0.38	0.53	12.79
<0.01	0.11	<0.01	<0.01	<0.01	0.01	0.02	0.02	0.03	0.01	0.02	0.07
55.97	44.05	56.36	56.72	56.66	56.45	56.79	56.03	26.80	15.13	56.69	19.53
0.69	0.33	0.73	0.71	0.64	0.49	0.67	0.51	0.04	24.50	0.69	0.00
<0.03	<0.03	<0.03	<0.03	<0.03	<0.03	<0.03	<0.03	<0.03	<0.03	<0.03	<0.03
<0.02	<0.02	<0.02	0.05	0.02	<0.02	0.02	0.03	<0.02	<0.02	<0.02	<0.02
100.59	100.29	100.81	100.65	98.70	100.39	100.65	99.91	99.98	100.15	101.37	99.91
4	4	4	4	4	4	4	4	4	6	4	4
1.001	0.994	1.002	0.996	0.970	0.995	0.990	0.970	0.004	1.693	0.998	0.004
0.001	0.001	0.002	—	0.001	0.001	0.002	—	0.006	0.057	0.001	0.003
0.015	0.020	0.007	0.007	0.006	0.005	0.008	0.009	1.807	0.469	0.006	1.978
0.002	0.005	0.001	0.001	0.002	0.003	0.001	0.004	0.174	0.010	0.002	0.010
0.006	0.317	0.006	0.004	0.009	0.010	0.007	0.040	0.025	0.011	0.010	0.269
—	0.002	—	—	—	0.000	0.000	0.000	0.001	0.000	0.000	0.002
1.946	1.644	1.957	1.972	2.020	1.970	1.978	1.985	0.981	0.817	1.960	0.732
0.017	0.009	0.018	0.018	0.016	0.012	0.017	0.013	0.001	0.951	0.017	0.000
—	—	—	—	—	—	—	—	—	—	—	—
—	—	—	0.001	0.001	—	0.001	0.001	—	—	—	—
2.989	2.992	2.992	2.999	3.025	2.998	3.003	3.022	2.999	4.009	2.995	2.999
0.3	15.9	0.3	0.2	0.5	0.5	0.3	2.0	—	—	0.5	—

crossed nicols. The mesostasis has a composition resembling that of alkali feldspar ($ab_{87}or_{13}$) with very low FeO (≈1.3 wt%). Notable is the extremely low CaO (<0.1 wt%) of the mesostasis, whereas the luminescent forsterite contains 0.56 wt% CaO.

A 20×50 μm melt inclusion with a shrinkage gas/vacuum bubble occurs within the core of one large refractory forsterite (Fig. 5A, arrow). The inclusion is glassy and has the same brownish tint as the mesostasis. The inclusion is very Na-rich (20 wt% Na_2O, 2.6 wt% K_2O) and has a composition closely matching that of nepheline. Most remarkable is the fact that the inclusion, albeit apparently entrapped in unaltered, FeO-poor forsterite, contains more Na than the surrounding mesostasis. Inclusion and mesostasis glass contain 0.8–1 wt% TiO_2. McSween (1977) reported a similar, FeO-poor (0.2 wt% FeO) and Na-rich (10.3 wt% Na_2O) inclusion in an isolated olivine grain from Kainsaz (CO3). The inclusion reported by McSween (1977), however, is richer in CaO (10.3 wt%) compared to 3.4 wt% CaO reported here.

Refractory cores and more fayalitic grains from DaG369/RF02 have similar oxygen isotope compositions and plot at $\delta^{18}O \approx -5‰$ between TFL and CCAM (Fig. 5B). The texture as well as the similar oxygen isotope ratios are consistent with in situ crystallization of the refractory cores and more fayalitic olivines in chondrule DaG369/RF02.

The lithic fragment DaG369/RF05 is composed of an irregularly shaped refractory olivine mantled by low-Ca pyroxene ($en_{89.0}fs_{9.5}wo_{1.5}$, Fig. 6A). The embayed contact between olivine and pyroxene indicates replacement of olivine by pyroxene. The core of the olivine exhibits CL-emission, whereas the rims and forsterite adjacent to cracks are too FeO-rich to show CL. The forsterite is not significantly enriched in ^{16}O and plots at $\Delta^{17}O = +2.5‰$ to the 'left' of the UOC field (Fig. 7).

Forsterite DaG369/RF06 is a large isolated refractory forsterite with uniform CL-emission in the core and a nonluminous ferrous rim (Fig. 6B). The thickness of the nonluminous rim varies between a few microns and a few tens of microns. An iron metal bleb occurs as an inclusion within the large forsterite, surrounded by a nonluminous halo. The halo probably formed due to oxidation of the metal during asteroidal alteration or during terrestrial weathering. The forsterite plots on the CCAM line and is significantly enriched in ^{16}O relative to ordinary chondrites ($\Delta^{17}O = -3.8‰$, Fig. 7).

3.3.3. *Dar al Gani 378 (H(L)3)*

Chondrule DaG378/RF03 is composed of porphyritic forsteritic olivine, which is embedded in a mesostasis that has a composition resembling that of alkali feldspar ($ab_{70}or_{30}an_{0.1}$, Fig. 8A), similar to that of DaG369/RF02, with low CaO and high TiO_2. The olivine with its embayed outline appears to be partially replaced by an assemblage of low-Ca pyroxene and glass (enlarged section, Fig. 8A).

The olivine grain consists of luminescent cores separated by ferrous altered fractures (Fig. 8A). The single luminescent core analyzed is not ^{16}O-rich and plots, together with one analysis of

Table 3. Oxygen isotope SIMS analyses of olivine and spinel from various unequilibrated chondrites. The oxygen isotope data are reported relative to the V-SMOW standard. The fayalite contents (mol%) and the CaO concentrations [wt.%] are also given.

Sample	No.	Grain	Phase	$\delta^{18}O$ (‰)	$\delta^{17}O$ (‰)	$\Delta^{17}O$ (‰)	*fa* (mol%)	CaO [wt%]
Chainpur	4	Cha/C1	*fo*	−15.3	−12.2	−4.2	0.38	0.69
Chainpur	5	Cha/C1	*spl*	−20.1	−20.5	−10.0	—	—
Chainpur	7	Cha/C1	*spl*	−21.0	−21.5	−10.5	—	—
Chainpur	9	Cha/C1	*fo*	−15.5	−15.3	−7.1	0.38	0.69
Chainpur	13	Cha/Iso01	*fa*	−16.4	−19.6	−11.0	n.d.	n.d.
Chainpur	14	Cha/Iso01	*fo*	−14.2	−17.5	−10.0	0.93	0.41
Chainpur	1	Cha1/C1	*fa*	7.7	−0.4	−4.5	0.68	0.11
Chainpur	2	Cha1/C1	*fo*	−1.4	1.0	1.7	0.50	0.52
Chainpur	3	Cha1/C1	*fa*	9.5	2.9	−2.1	0.68	0.11
Chainpur	1	Cha1/Iso01	*fo*	1.6	1.8	0.9	0.56	0.58
DaG013	1	DaG013/RF08	*fo*	−21.1	−15.8	−4.7	0.35	0.68
DaG013	2	DaG013/RF08	*fo*	−22.1	−14.9	−3.3	0.35	0.68
DaG013	3	DaG013/RF08	*fa*	−7.3	−4.5	−0.7	11.40	0.13
DaG013	1	DaG013/RF10	*fo*	−18.0	−15.9	−6.5	0.36	0.66
DaG013	2	DaG013/RF10	*fa*	−7.9	−5.3	−1.1	5.34	0.25
DaG378	1	DaG378/RF05	*fo*	−10.4	−10.0	−4.5	1.74	0.49
DaG378	2	DaG378/BO	*fa*	2.8	1.7	0.3	34.12	0.05
DaG378	1	DaG378/RF03	*fo*	1.6	3.2	2.3	0.73	0.48
DaG369	2	DaG369/RF02	*fo*	−7.5	−5.2	−1.3	0.37	0.56
DaG369	3	DaG369/RF02	*fa*	−3.9	−5.5	−3.4	25.10	0.19
DaG369	5	DaG369/RF02	*fo*	−5.4	−2.0	0.8	0.37	0.56
DaG369	6	DaG369/RF02	*fo*	−4.8	−1.7	0.8	0.37	0.56
DaG369	9	DaG369/RF02	*fa*	−5.6	−1.2	1.8	25.10	0.19
DaG369	1	DaG369/RF05	*fo*	−1.0	1.9	2.5	0.45	0.41
DaG369	1	DaG369/RF06	*fo*	−0.1	−3.9	−3.8	0.31	0.67
Murchison	1	Mur/RF07	*fo*	−6.7	−4.0	−0.5	2.0	0.45
Murchison	2	Mur/RF07	*spl*	0.5	−4.8	−5.1	—	—
Murchison	1	Mur/RF05	*fo*	−11.1	−14.6	−8.8	0.34	0.67
Renazzo	2	Ren/RF06	*fo*	1.8	−3.3	−4.3	0.52	0.49
Allende	1	All/RF03	*fo*	−5.0	−8.4	−5.7	0.48	0.67
Allende	3	All/RF03	*fa*	−7.6	−5.3	−1.3	29.22	0.11
Allende	1	All/RF07	*fo*	−11.0	−12.8	−7.0	0.29	0.69
Allende	2	All/RF07	*fa*	−6.7	−8.6	−5.1	15.86	0.33
Allende	1	All/RF11	*fo*	−7.7	−9.8	−5.8	0.28	0.73
Allende	1	All/RF16	*fo*	−10.9	−10.9	−5.2	0.20	0.71
Allende	2	All/RF16	*fo*	−6.4	−7.7	−4.3	0.20	0.71
Allende	1	All/S01	*fo*	−10.5	−9.8	−4.3	0.47	0.61

an olivine bar from a neighboring barred olivine chondrule (DaG378/BO) in the field of ordinary chondrites (Fig. 9).

DaG378/RF05 is a Na-, Al-rich type-IA porphyritic olivine chondrule consisting of olivine and Na-, Al-rich mesostasis (Fig. 8B). The opaque phases are troilite and Fe, Ni-metal which are partly oxidized, probably during terrestrial weathering. Only a few of the olivine grains have preserved the luminescence in their cores. The mesostasis has a composition resembling that of alkali feldspar ($ab_{85}or_{15}an_{<0.1}$). As in DaG369/RF02 and DaG378/RF03, CaO is notably low (<0.5 wt%) in the interstitial mesostasis. The oxygen isotope ratio of the luminescent forsterite core shows a significant enrichment in ^{16}O relative to unequilibrated ordinary chondrites ($\Delta^{17}O = -4.5‰$) and plots near the Y&R slope-1.0 mixing line (Fig. 9). All olivine grains from DaG378/RF05 appear to have crystallized in situ within the chondrule.

3.3.4. Renazzo (CR2) and Murchison (CM2)

Porphyritic type-IA chondrule Ren/RF06 from Renazzo (Figs. 10A,B) very much resembles chondrule Cha1/C1 from Chainpur (Figs. 2C,D). The chondrule consists of porphyritic olivine ($fa_{0.5}$) and Ni-, Cr- and Si-rich iron metal blebs (6 wt% Ni, 1.4 wt% Cr, 0.5 wt% Si, Schönbeck, unpublished data). Forsterites from the outer part of Ren/RF06 exhibit CL-emission, whereas grains from the interior are nonluminous. Similarly to Cha1/C1, some forsterites exhibit inverse CL-zoning with an overall low CL-intensity. A single luminescent forsterite was measured from Ren/RF06 (Fig. 10B). The forsterite is slightly enriched in ^{16}O relative to the Renazzo parent body ($\Delta^{17}O = -4.3‰$, Fig. 11A, bulk and matrix data from Clayton and Mayeda, 1999) and plots on the CCAM. Ren/RF06 is slightly more ^{16}O-rich than the most ^{16}O-rich chondrules from CR chondrites (bulk CR chondrule data from Weisberg et al., 1993).

Refractory forsterite Mur/RF05 is euhedrally shaped and ≈300 μm across. The forsterite is highly luminescent throughout, with no ferrous rim (Figs. 10C,D). Fragments of the large grain were broken off during preparation of the polished thin section. The extremely sharp contact between forsterite and the hydrous Murchison matrix is notable. Bischoff (1998), in his review article, suggested that such features are evidence against extensive late-stage, postaccretionary hydrous alteration. The distance between the ferroan matrix olivine grain

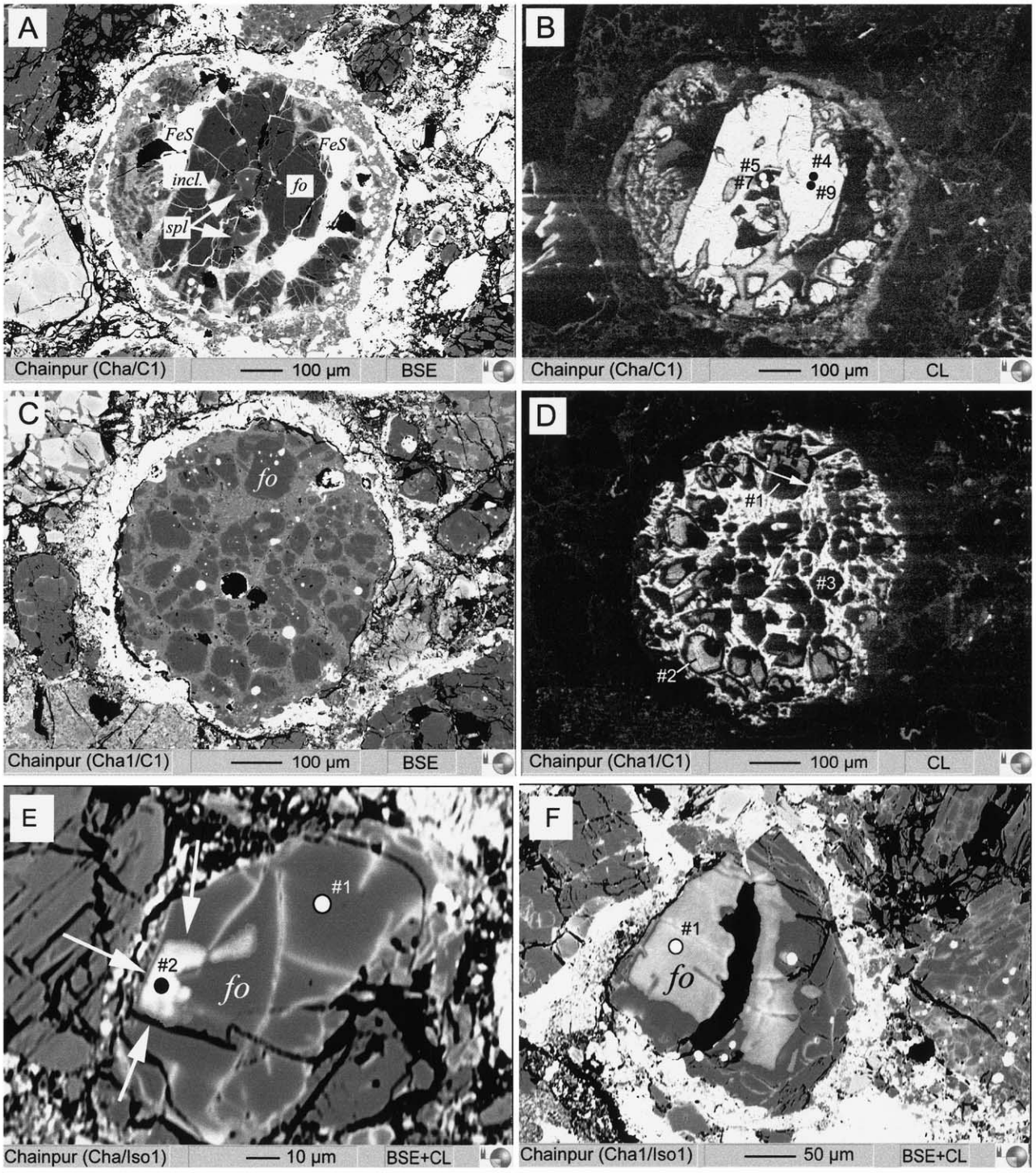

Fig. 2. Refractory forsterite grains from Chainpur (LL3.4). Numbers refer to ion probe analyses (Table 3). (A, B) Macroporphyritic, spinel bearing chondrule Cha/C1 with a single forsterite grain that is embedded in a fine grained calcic mesostasis. The opaque phase is troilite (FeS). (C, D) Porphyritic type-IA chondrule Cha1/C1 with luminescent forsterites in a fine grained calcic mesostasis. The CL-image reveals unusual inverse zoning (i.e., nonluminous cores are overgrown by luminescent rims) of forsterites in the outer part of the chondrule. (E) Isolated refractory forsterites grain Cha/Iso1 with a small luminescent area (arrows). (F) Fragmented refractory forsterite grain Cha1/Iso1.

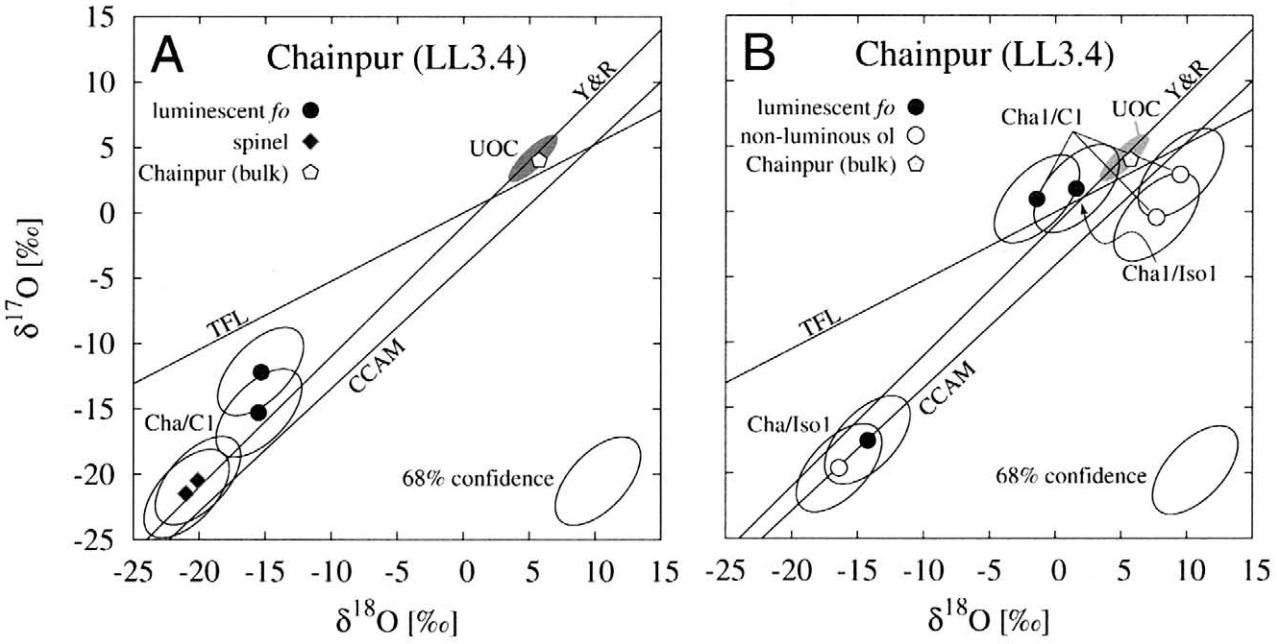

Fig. 3. (A) O-isotope ratios of minerals in spinel-bearing chondrule Cha/C1. (B) Isotope ratios of two isolated refractory forsterites (Cha/Iso1, Cha1/Iso1) and analyses obtained on olivines from type-IA chondrule Cha1/C1. Bulk oxygen isotopic compositions of Chainpur and other OCs are taken from Clayton et al. (1991).

and the FeO-poor refractory forsterite Mur/RF05 is only ≈20 μm (detail in Fig. 10C). Heterogeneities in the water activity on such a small scale on a parent body are not very likely to have occurred. It is therefore concluded that the ferroan olivine did not gain its FeO in situ during late-stage parent body alteration. The nonferrous rim of Mur/RF05 would not have been preserved during extensive hydrous alteration.

Refractory forsterite Mur/RF05 is highly enriched in ^{16}O relative to the Murchison bulk composition and plots on the CCAM line (Fig. 11B).

Mur/RF07 is an isolated forsteritic olivine grain which is too high in FeO (2 wt%) to show CL emission (Steele, 1986a). Despite of its nonrefractory composition it was chosen for SIMS analyses since it contains two refractory inclusions of two refractory minerals: one of FeO-poor spinel ($Mg_{0.98}Fe_{0.03}Al_{1.81}Cr_{0.17}O_4$) and the other of FeO-poor Al-, Ti-rich diopside ($Ca_{0.95}Mg_{0.82}Fe_{0.01}Al_{0.47}Cr_{0.01}Si_{1.69}Ti_{0.06}O_6$, Fig. 10E).

The forsterite host and the spinel inclusion are both not significantly enriched in ^{16}O (Fig. 11B). The spinel inclusion plots on the CCAM line, whereas the forsterite plots towards lower $\delta^{18}O$. Using the olivine/spinel O-isotope fractionation data of Zheng (1991, 1993, quartz-mineral), at 1000°C, forsterite should be ≈1‰ higher in $\delta^{18}O$ than coexisting spinel. Even at higher temperatures, forsterite in equilibrium with spinel should be enriched in the heavy isotopes. The measured depletion of forsterite in ^{18}O relative to spinel, therefore, cannot be due to mass-dependent fractionation and is probably due to analytical uncertainties.

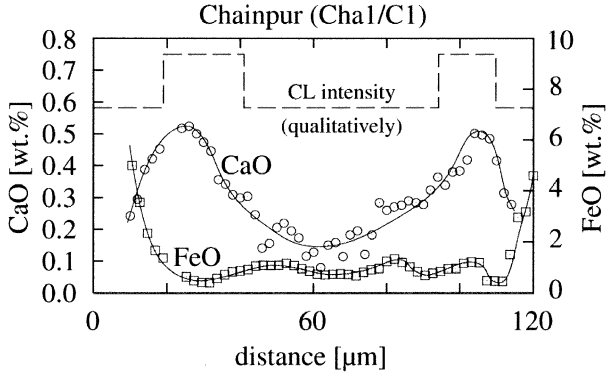

Fig. 4. Chemical profile measured across an inversely zoned forsterite from Cha1/C1 (see Fig. 2D). The zone with CL emission is characterized by enhanced CaO, whereas the nonluminous zone is poor in CaO.

3.3.5. *Allende (CV3)*

The isolated refractory forsterite grain All/RF03 is ~100 μm across and is embedded in the fine-grained Allende matrix (Fig. 12A). Its outer grain boundary is fayalite rich (fa_{30}) and poor in Ca and Al. Two spots were analyzed for oxygen, one located in the refractory core and a second spot at the outer, FeO-rich margin (Fig. 12A). The refractory core ($\Delta^{17}O = -5.7‰$) and the fayalitic rim ($\Delta^{17}O = -1.3‰$) are both only slightly enriched in ^{16}O relative to the Allende parent body (Fig. 13), but not enriched relative to CV3 chondrules (data from Clayton et al., 1983; Jones et al., 2000b).

All/RF07 is a large chondrule fragment that hosts a single, ≈100 μm-sized luminescent forsterite (Fig. 12B). The interstitial mesostasis is rich in calcic plagioclase ($\approx an_{80}$). One spot in

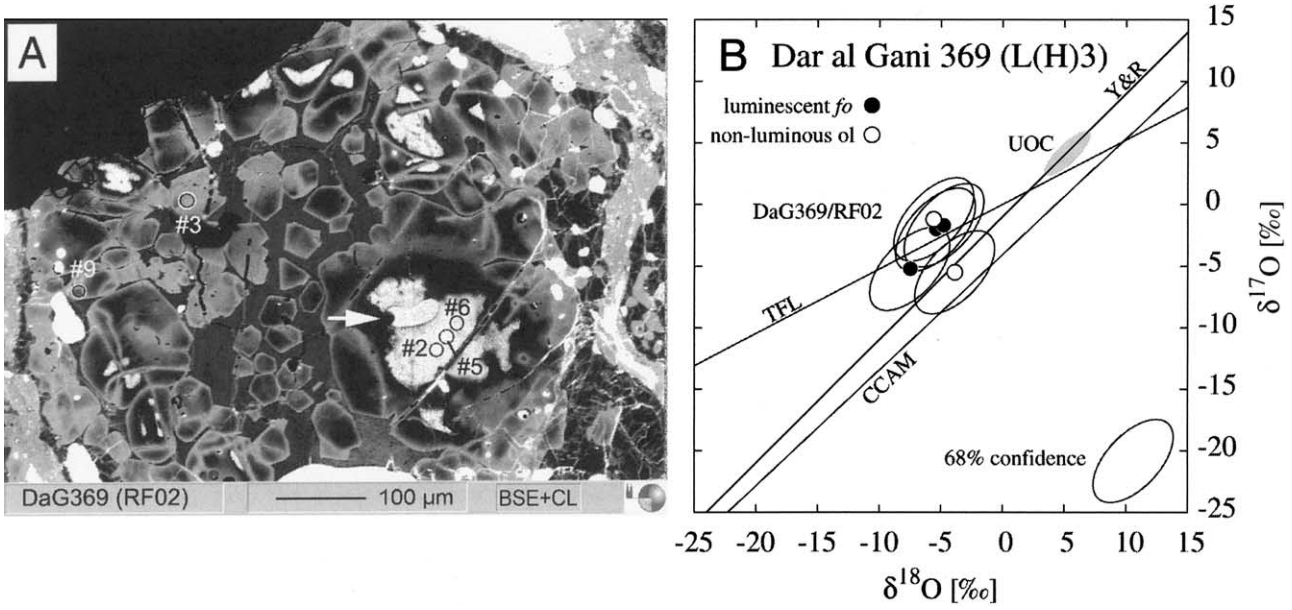

Fig. 5. (A) Na, Al-rich chondrule (DaG369/RF02) from Dar al Gani 369. Porphyritic olivine is embedded in a vitreous mesostasis. The large refractory forsterite phenocryst contains a melt inclusion with shrinkage bubble (arrow). The locations of ion probe spots are indicated. (B) Plot illustrating the oxygen isotope ratios of forsterite and more fayalitic olivine from chondrule DaG369/RF02.

the refractory core and one on a fayalitic olivine (fa_{10-15}) were chosen for SIMS analyses. The refractory core is significantly enriched in ^{16}O relative to the fayalite rich olivine of chondrule fragment All/RF07. The refractory core and fayalitic olivine are both not enriched in ^{16}O relative to CV3 chondrules and plot on an ^{16}O exchange trajectory between Y&R and CCAM lines (Fig. 13).

Chondrule All/RF11 is a porphyritic olivine chondrule containing abundant luminescent forsterites, which are rimmed by fayalitic olivine (Fig. 12C). The fayalitic rims are less enriched in refractory lithophile components and reach FeO contents of 33 wt%. The analyzed forsteritic core is slightly enriched in ^{16}O having $\Delta^{17}O = -5.8‰$. All/RF11 plots towards the 'left' of the CCAM line, close to the Y&R mixing line (Fig. 13).

Refractory forsterite All/RF16 is ~500 μm across and shows uniform bright CL-emission in the core (Fig. 12D). The grain is cross-cut by veinlets filled with material rich in Si, Al and Na ($Na_2O \leq 20$ wt%). Individual phases could not be identified, but strong enrichment in Na indicates the presence of albite and/or nepheline. CaO and Al_2O_3 in the forsterite decrease

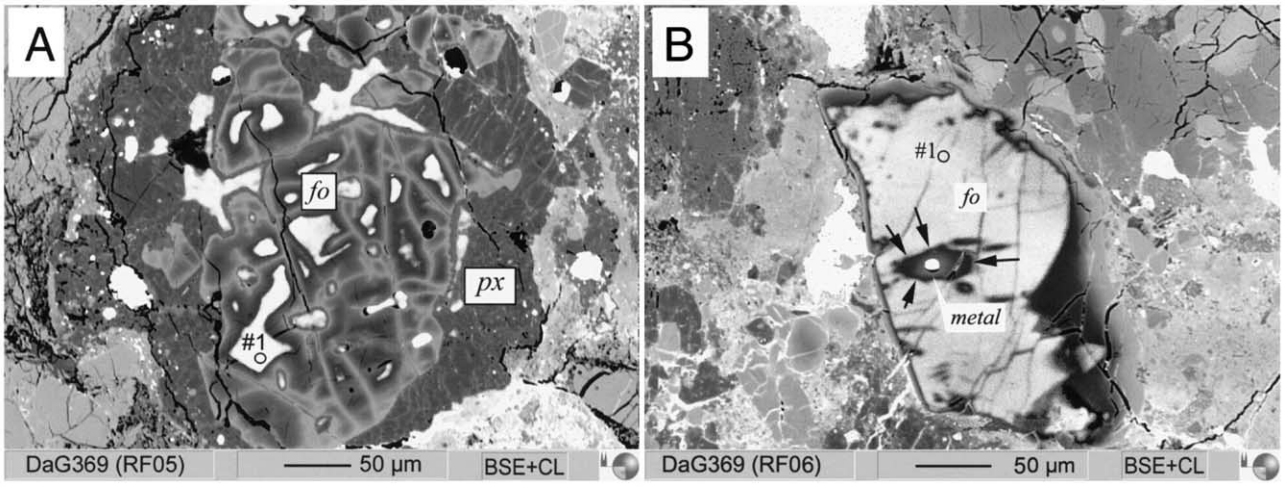

Fig. 6. Lithic fragment DaG369/RF05 and isolated refractory forsterite DaG369/RF06. The positions of ion probe spots are indicated. (A) Forsterite DaG369/RF05 is enriched in Fe along abundant fractures and is surrounded by a mantle of pyroxene, replacing olivine. (B) Isolated refractory forsterite DaG369/RF06 consists of a large luminescent core with an asymmetric nonluminous rim (left rim vs. right rim). Note the nonluminous halo around the iron metal inclusion in Da369/RF06 (arrows).

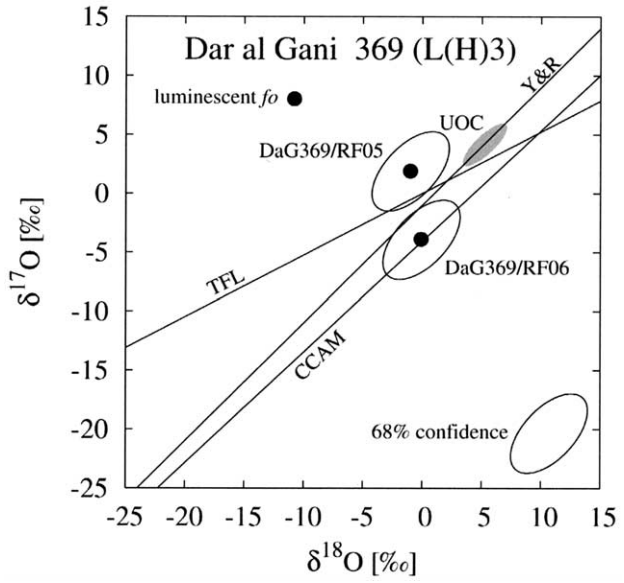

Fig. 7. Oxygen isotope ratios of isolated refractory forsterites DaG369/RF05 and DaG369/RF06 from Dar al Gani 369.

from core (0.7 wt% CaO) towards the outer, more FeO-rich rim (0.25 wt% CaO). Two spots were analyzed on the refractory core of All/RF16. Both analyses plot on the Y&R mixing line at $\delta^{18}O \approx -8‰$ (Fig. 13).

Chondrule All/RF0S is a porphyritic type-IA chondrule, which consists of olivine with luminescent forsterite-rich cores (Fig. 12E). The forsterite is slightly enriched in ^{16}O relative to bulk Allende and plots between the Y&R and CCAM lines at $\delta^{18}O = -10‰$.

3.3.6. Dar al Gani 013 (R-Chondrite, R3.5–6)

R-chondrites are the most oxidized group of chondrites with the highest $\Delta^{17}O$ values ($\Delta^{17}O \approx +3‰$, Schulze et al., 1994; Jäckel et al., 1996; Bischoff, 2000; Greenwood et al., 2000). Dar al Gani 013 is a brecciated R-chondrite with clasts of unequilibrated type-3 lithologies (Bischoff, 2000). The oxygen isotope ratios of Dar al Gani 013 (bulk) were determined by Jäckel et al. (1996) as $\delta^{17}O = +5.38‰$ and $\delta^{18}O = +5.88‰$ with $\Delta^{17}O = +2.3‰$. The matrix olivines have a composition of 40–44 mol% fayalite. For a more detailed petrological description of Dar al Gani 013, see Bischoff (2000).

Refractory forsterite DaG013/RF08 is approximately 70 μm in the short dimension and is isolated in the fine grained fayalite rich matrix (Fig. 14A). The refractory core is rimmed by nonrefractory, $\approx$10 μm-thick fayalitic olivine. The FeO content increases up to 34 wt% towards the contact with the FeO-rich matrix. Concentrations of RLEs are low in the fayalitic rim.

CL-microscopy reveals a zone of unusual bright CL-emission, which is approximately 5$\times$30 μm wide (Fig. 14A). The increase in CL-intensity correlates with a strong increase in Al_2O_3 (0.2–0.3 $\rightarrow$ 0.6 wt%) and TiO_2 ($\sim$0.05 $\rightarrow$ 0.1 wt%) from 'normal' refractory forsterite to the 'high-CL zone' (Fig. 15A). The increase in Al_2O_3 and TiO_2 does not correlate with an increase in Cr_2O_3 as one would expect from the presence of Cr-spinel (e.g., Weinbruch et al., 1990). If the zone high in Al_2O_3 contains dispersed Cr-free Mg-spinel inclusions, these must be extremely small since they were not resolved BSE-microscopy. The transition from Al-poor to Al-rich occurs over $\approx$5.5 μm. The actual gradient in Al may, however, be even steeper. Phase boundary fluorescence effects make detection of μm-wide compositional gradients using EPMA impossible. Concentrations of TiO_2, Al_2O_3 and CaO decrease towards the more fayalitic rims to 'normal' values for fayalitic olivine. The FeO profile shows an abrupt increase at 50 μm in radius (Fig. 15A). The sharp compositional contact between refractory core and ferrous rim indicates formation of the rim through fayalite overgrowth rather than by diffusional exchange with the ferrous matrix. Formation of the fayalite rim as overgrowth is also

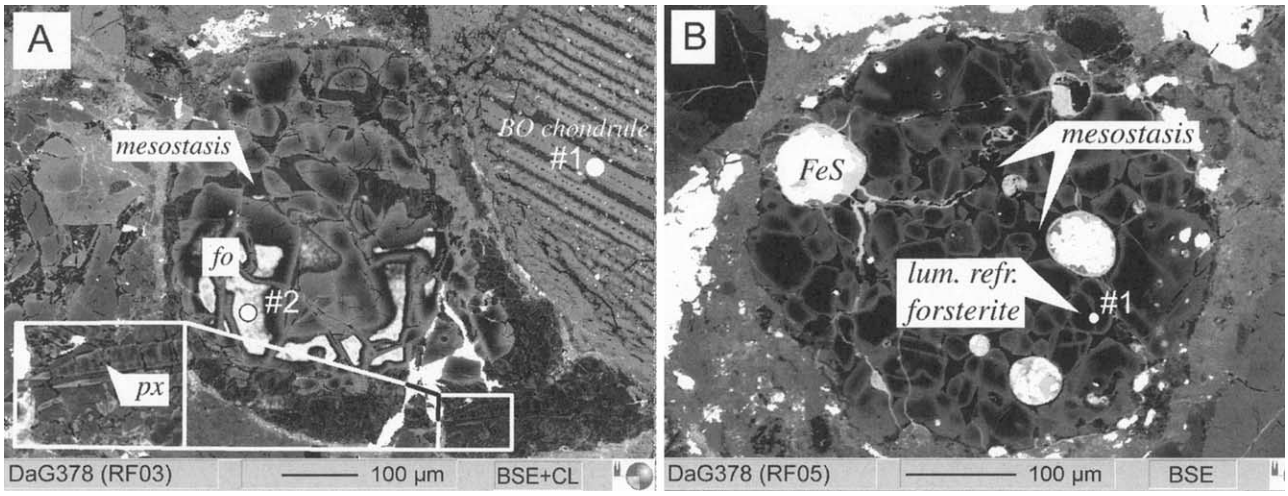

Fig. 8. (A) Porphyritic Na-, Al-rich chondrule DaG378/RF03. Refractory, partially luminescent forsterite is embedded in a sodic alkali feldspar rich mesostasis. Low-Ca pyroxene occurs to the bottom right of the chondrule. Analysis 1 (DaG378/BO) is located on an olivine bar from the neighboring BO chondrule and analysis 2 in the core of a luminescent forsterite (DaG378/RF03). (B) Na-, Al-rich chondrule DaG378/RF05 with forsteritic olivine, fine grained sodic mesostasis and partially altered troilite.

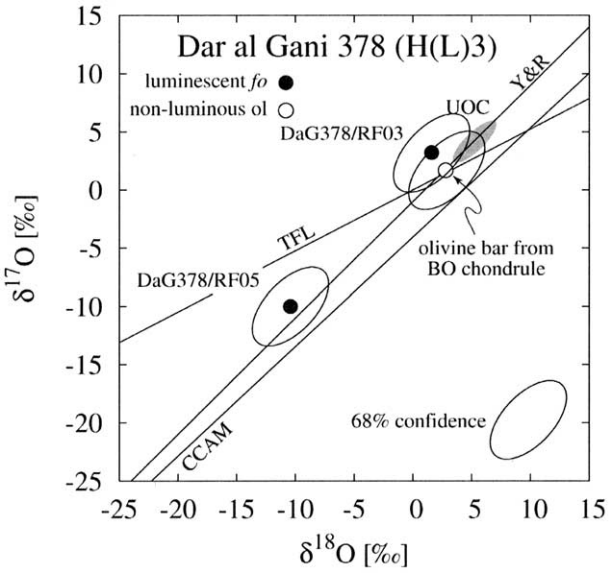

Fig. 9. Oxygen isotope ratios of refractory forsterite grains and a single barred olivine from Dar al Gani 378. Only DaG378/RF05 is significantly enriched in ^{16}O relative to ordinary chondrites.

indicated by the facetted outer margin of DaG013/RF08 (enlarged section, Fig. 14A).

Refractory forsterite DaG013/RF10 is an irregularly shaped, embayed ≈50×100 μm forsterite with a homogeneous cathodoluminescent FeO-poor core and a fayalitic rim (Fig. 14B). CaO and Al_2O_3 (0.4 wt%) are high in the core and abruptly decrease towards the fayalitic rim. The fayalitic rim is nonrefractory with FeO-contents increasing towards the matrix contact up to ≈34 wt%.

The contacts between forsteritic cores and ferrous rims of refractory forsterites DaG013/RF08 and DaG013/RF10 are characterized by Cr- and Al-rich layers (Figs. 15A,B). The peaks of Al and Cr are displaced by a few microns and do not entirely overlap. This indicates that the Cr-, Al-rich layers are zoned, with probably Al-rich spinel dominating the inner most part of the layers and Cr-rich spinel occurring at the outer part. The occurrence of Cr-rich spinel inclusions in association with ferrous rims on forsteritic olivines from Allende was described by Peck and Wood (1987) and Weinbruch et al. (1990).

The refractory cores of DaG013/RF08 and DaG013/RF10 are enriched in ^{16}O by $\Delta^{17}O$ between −6 and −10‰ relative to the host meteorite (Fig. 16). No difference in oxygen isotope ratios can be discerned between the refractory core and the high-Al zone within the core in DaG013/RF08. The core of DaG013/RF10 shows a similar enrichment in ^{16}O as the core of DaG013/RF08 (Fig. 16). The cores plot to the 'left' of the Y&R mixing line in the $\delta^{17}O$ vs. $\delta^{18}O$ diagram. The small spot size of the TiTech ion probe allowed us to determine the oxygen isotope ratio of the outermost fayalitic rim around the forsterites DaG013/RF08 and DaG013/RF10. Both rims are less depleted in ^{16}O and plot on the Y&R line (Fig. 16), but are still significantly enriched relative to the R-chondrite parent body by $\Delta^{17}O \approx -2$‰.

The refractory cores as well as the fayalitic rims plot along a slope 0.8 mixing line in the $\delta^{17}O$ vs. $\delta^{18}O$ diagram ('RML', Fig. 16). The bulk composition of Dar al Gani 013 as well as fayalitic olivines from R-chondrite PCA91241 plot on the upper extension of the slope 0.8 line. Magnetite from R-chondrite PCA91214 plots above the TFL at $\delta^{18}O \approx -13$‰ (Greenwood et al., 2000; Fig. 16). The O-isotopic composition of the magnetite was established during its formation on the R-chondrite parent body and was shifted by mass-dependent fractionation along the R-chondrite mass fractionation line ('RML', Fig. 16 towards lower $\delta^{18}O$).

4. DISCUSSION

4.1. Widespread Occurrence of Refractory Forsterites

Refractory forsterite is a widespread component of UOCs and CCs with concentrations ranging up to 0.35 vol%. There is no apparent difference in abundance of refractory forsterites between UOCs and CCs (Table 1). Refractory forsterites are also present in two sections of R-chondrite Dar al Gani 013 with concentrations of 0.003 and 0.03 vol%, respectively (Table 1). The occurrence of refractory forsterites appears to be neither related to the chemistry nor the oxidation state of the host meteorite. Even the most oxidized R-chondrites contain FeO-poor, refractory forsterites (Weisberg et al., 1991; Schulze et al., 1994; Bischoff, 2000).

4.2. Chemical Composition of Refractory Forsterites

Based on their composition, we group forsteritic olivine from the various groups of chondrites into a) highly refractory (>0.6 wt% CaO), b) moderately refractory (0.3–0.6 wt% CaO) and c) nonrefractory forsterite with <0.3 wt% CaO. Highly refractory forsterites are present in UOCs, CCs and RCs. If highly refractory forsterites, similar to nonrefractory olivine, crystallized from chondrule melts, these melts must have been extremely RLE-rich with ≈21 wt% CaO (Weinbruch et al., 2000; Klerner et al., 2000; Pack et al., 2003). A CaO content of ≈21 wt% is, however, is significantly above the CaO contents of chondrules that rarely exceed 5 wt% CaO (Gooding et al., 1983; Grossman and Wasson, 1983; Rubin and Wasson, 1987; Jones and Scott, 1989; Palme et al., 1992).

The Al_2O_3 contents of refractory forsterites vary between 0.1 and 0.6 wt% with a typical CaO/Al_2O_3-ratio of 2–3 (Table 2). Again there is no systematic difference between refractory forsterites from CCs and UOCs or RCs. Using partitioning data from Agee and Walker (1990) for Al and from Libourel (1999) for Ca, the CaO/Al_2O_3-ratio and the Ca and Al concentrations are indicative of equilibration with a refractory melt with chondritic Ca/Al. Klerner et al. (2000) suggest the host melt of highly refractory forsterites was uniformly enriched in RLEs (Ca, Al, Sc, Yb) by 10–20×C1. Pack et al. (2003) have shown that refractory forsterites from different types of chondrites (OC, CC, RC) have very similar minor and trace element contents with fractionated RLEs, including REEs, indicative of equilibration with a silicate melt uniformly enriched in RLEs by ~10–20×C1.

Based on these observations, we exclude formation of refractory forsterites from type-I chondrules as advocated by McSween (1977), Roedder (1981), Jones (1992, 1996) and Leshin et al. (1997). Hence, highly refractory forsterites in type-I chondrules are xenocrysts. The size of refractory forster-

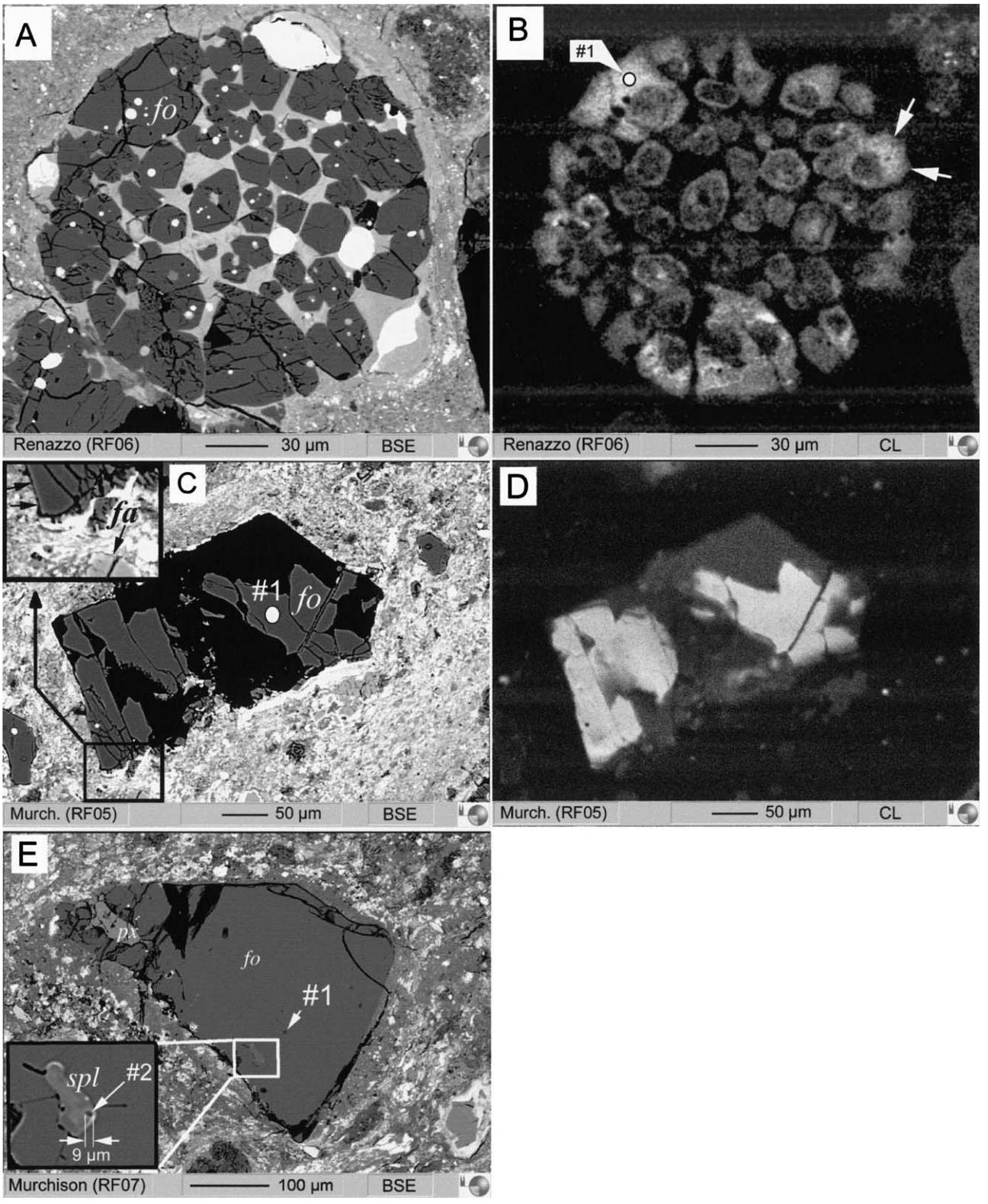

Fig. 10. (A) Type-IA chondrule Ren/RF06 from Renazzo with porphyritic forsterite and Ni-, Cr- and Si-rich iron metal. (B) CL image of Ren/RF06 showing the weak overall CL intensity of the forsterites with partially inverse CL zoning (arrow, see also Fig. 2D). The position of the ion probe spot in a luminescent olivine is indicated. (C) BSE image and (D) CL image of a large, highly luminescent isolated refractory forsterite grain (Mur/RF05) from Murchison. Note the euhedral outline and the sharp contact between the unaltered forsterite and the hydrous matrix containing fayalitic olivine (arrows, enlarged image, top left). Parts of the grain were broken off during preparation of the thin section (black area). (E) BSE image of an isolated nonluminous forsterite Mur/RF07 with a spinel and a high-Ca pyroxene inclusion. Positions of ion probe spots are indicated.

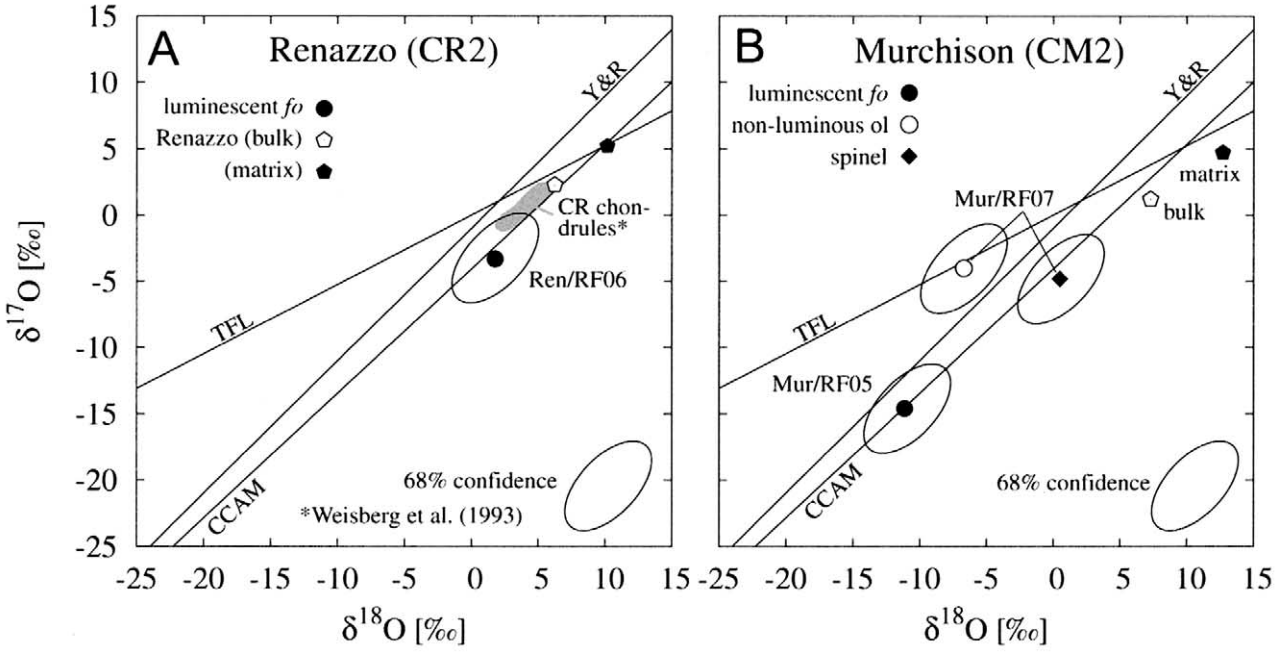

Fig. 11. (A) Oxygen isotope ratios of refractory chondrule olivine (Ren/RF06), Renazzo matrix and bulk data (Clayton and Mayeda, 1999). The gray shaded area outlines CR chondrule data from Weisberg et al. (1993). (B) O-isotopic composition of an isolated refractory forsterite (Mur/RF05) and a nonluminous isolated forsterite with spinel inclusion (Mur/RF07) from Murchison (CM2).

ites up to several hundreds of microns along with the RLE fractionation (Klerner et al., 2000; Pack et al., 2003) and the occurrence of melt inclusions, however, suggests an igneous origin of refractory forsterites. Condensed silicates are assumed to be very fine grained with grain sizes in the micron and submicron range (Blum and Munch, 1993).

The CaO contents of chondritic, FeO-poor (<10 wt%) olivines anticorrelate with the FeO content (Leshin et al., 1997; McSween, 1977; Brearley and Jones, 1998; Fig. 17, gray shaded area). Refractory forsterites along with their fayalitic, nonrefractory rims follow the same trend of decreasing CaO with increasing FeO (Fig. 17). The data sets by McSween (1977) and Brearley and Jones (1998) include data on highly refractory forsterites which, according to the authors, are derived from type-I chondrules. The relation is reversed for FeO contents exceeding ≈10 wt%, which can be explained by enhanced incorporation of Ca into more ferrous olivine compared to forsterite (Libourel, 1999). The gradual variation of CaO and FeO from the highly refractory end member towards nonrefractory, ferrous olivines indicates that highly refractory forsterites and common, nonrefractory olivines formed by a single process, i.e., crystallization from a liquid.

4.3. Open System, Fractional Crystallization (OSFC) Model

We have demonstrated that highly refractory forsterites show evidence for an igneous origin. The host melts parental to the highly refractory forsterites, however, must have been much more refractory than most chondrules. We suggest that the refractory melts formed by gas-liquid condensation (see Pack and Palme, 2003). Equilibrium condensation calculations of Grossman (1972), Yoneda and Grossman (1995) and Ebel and Grossman (2000) show that at a solar dust/gas ratio (D/G) and a total pressure (p^{tot}) of $<10^{-3}$, only refractory oxides and silicates are stable condensates. Condensation temperatures generally increase with increasing p^{tot} and/or increasing D/G, to values where partial melts become stable (Yoneda and Grossman, 1995; Ebel and Grossman, 2000). Yoneda and Grossman (1995) calculated the stabilities of CMAS melts at various p^{tot} and different D/Gs using the Berman (1983) nonideal solution model. Ebel and Grossman (2000) used the multicomponent MELTS nonideal thermodynamic model by Ghiorso and Sack (1995), to treat FeO-bearing liquids.

The calculated melt condensates are rich in CaO and Al_2O_3 and should also be rich in other RLEs that condense at high temperatures, e.g., Sc, Ti, REEs. The concentration of FeO in the melt condensates depends on the ambient oxygen fugacity (i.e., the D/G) as well as on p^{tot}. At solar D/G O/H = 4.9×10^{-4}, (Palme and Beer, 1993) and a $p^{tot} = 10^{-6}$ bar, Fe condenses as Fe, Ni-alloy and only very little FeO condenses into oxides, silicates and silicate melts (e.g., Palme and Fegley, 1990; Ebel and Grossman, 2000). At D/G = 1000×solar and $p^{tot} = 10^{-3}$ bar up to 26 wt% FeO is in the liquid.

Early phases to crystallize from such melt condensates are perovskite, spinel and forsterite. We suggest that highly refractory forsterites formed by open system, fractional crystallization (OSFC, see also Pack and Palme, 2003) in such RLE-rich melt condensates (Fig. 18). The first forsterite that crystallizes in a condensed melt droplet (D/G = 100×solar, $p^{tot} \approx 10^{-3}$ bar, 1782 K, Ebel and Grossman, 2000) contains 0.34 wt% CaO and 0.25 wt% FeO. The CaO concentration of the forster-

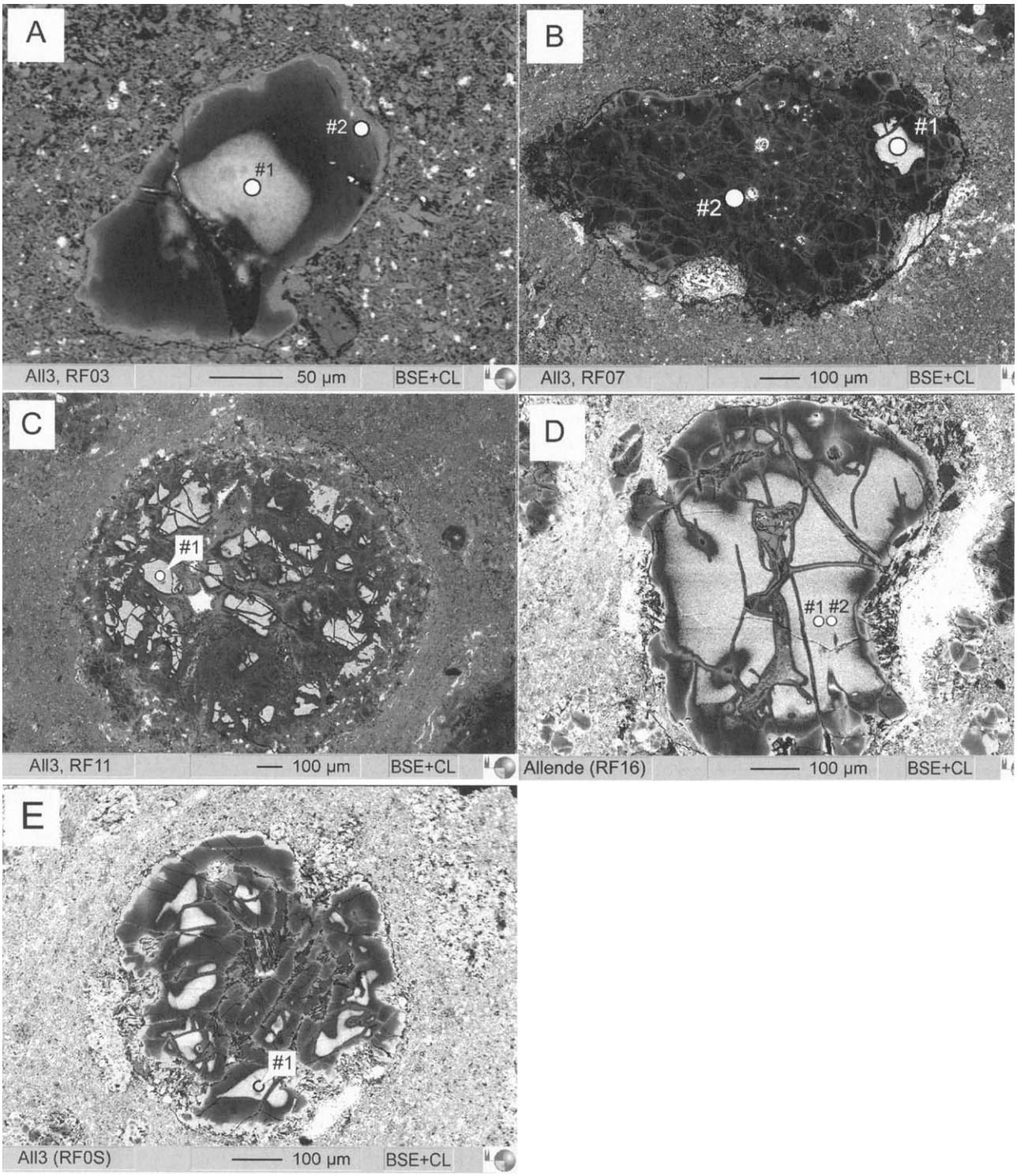

Fig. 12. Refractory forsterites from Allende with positions of ion spots indicated. (A) Isolated refractory forsterite grain All/RF03 with a luminescent core in the center of the grain. (B) Chondrule fragment All/RF07 with a single luminescent forsterite. (C) Porphyritic chondrule All/RF11 with abundant luminescent refractory forsterite cores. (D) Large isolated refractory forsterite grain All/RF16. The forsterite is cross-cut by veinlets, which are filled with alkali-rich material. (E) Chondrule All/RF0S with luminescent forsteritic olivine cores.

ite was calculated using Ca-partitioning data by Libourel (1999), whereas the FeO content was taken from Ebel and Grossman (2000). The CaO content of 0.73 wt% as given by Ebel and Grossman (2000) seems to be an overestimate that may be related to the uncertainty in CaO-activity models that were used for forsterite and melt. At the temperature at which

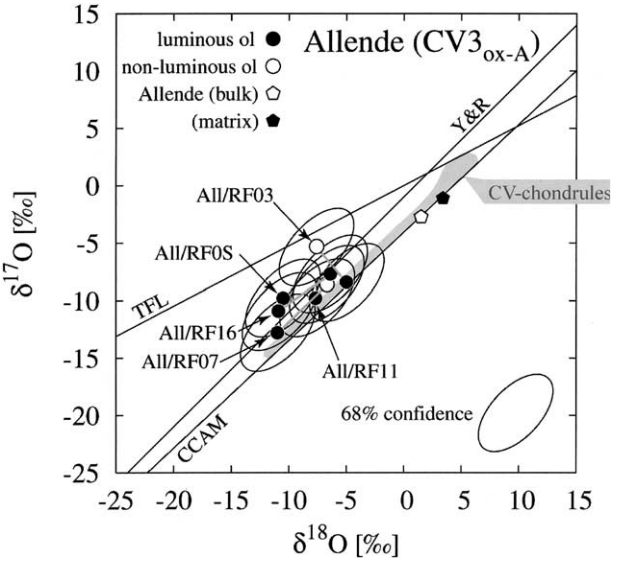

Fig. 13. Plot illustrating the O-isotope ratios of refractory forsterites and fayalitic rims from Allende. The 'CV chondrule field' (gray shaded area) is defined by data of Clayton et al. (1983) and Jones et al. (2000b).

forsterite appears, the CaO concentration of the melt decreases with increasing D/G. Therefore, a D/G <100 may result in a CaO concentration in the melt sufficiently high ($\sim$20 wt%) to coexist with refractory forsterite with 0.7 wt% CaO.

Although we suggest formation of refractory forsterites in melt condensates with D/G $<100\times$solar, we will discuss the crystallization sequence in detail using the results for D/G = $100\times$solar and $p^{tot} = 10^{-3}$ bar, as calculated by Ebel and Grossman (2000, their figs. 6 and 10). Spinel inclusions in highly refractory forsterites (Figs. 1A,B, 2A,B) can be explained in this model as relicts of an earlier spinel population, which coexisted with the melt at higher temperatures (Fig. 18). The stability of spinel and forsterite overlaps by $\approx$100 K, so that forsterite may entrap spinel during early growth (Ebel and Grossman, 2000, their fig. 6). With decreasing temperature, spinel becomes unstable relative to melt, and early-formed spinel grains will be dissolved. The decomposition of the spinel, and also the decomposition of perovskite, is the result of decreasing temperature, which is accompanied by a change in melt composition from highly refractory towards more siliceous (Ebel and Grossman, 2000). In contrast to spinel, inclusions of perovskite were not observed within refractory forsterites. According to Ebel and Grossman (2000), perovskite is resorbed $\sim$20 K above the forsterite appearance temperature at 1782 K. Therefore, no perovskite is present at the time of forsterite crystallization. Ebel noted in his review that the perovskite stability field could also be an artifact of the condensation calculations which require a Ti-bearing phase.

A characteristic of refractory forsterites from different types of chondrites is the trend of decreasing CaO from the core towards the more ferrous rim (Fig. 1C; Jones, 1992, their figs. 6a and 7b). This trend is opposite to what is expected in a closed igneous system, such as chondrule melts. Crystallization of olivine in a chondrule inevitably leads to enrichment of CaO in the residual melt. Libourel (1999) demonstrated that elevated fayalite contents of olivine along with increasing CaO contents in the residual melt lead to an increase of the olivine/melt Ca-partitioning. These two effects along with the apparent temperature independence of the Ca olivine to melt partitioning (Libourel, 1999) would even produce a pronounced increase in Ca towards the more ferrous rims. An example for "normal" igneous zoning is shown in Figure 4. The decrease of CaO in the outermost few microns of the phenocryst has probably been established during mild parent body metamorphism.

Melt condensates differ from chondrules in that they are chemically open systems. Chondrules that form by flash heating of a solid precursor material are, to a first approximation, chemically closed systems. The composition of melt conden-

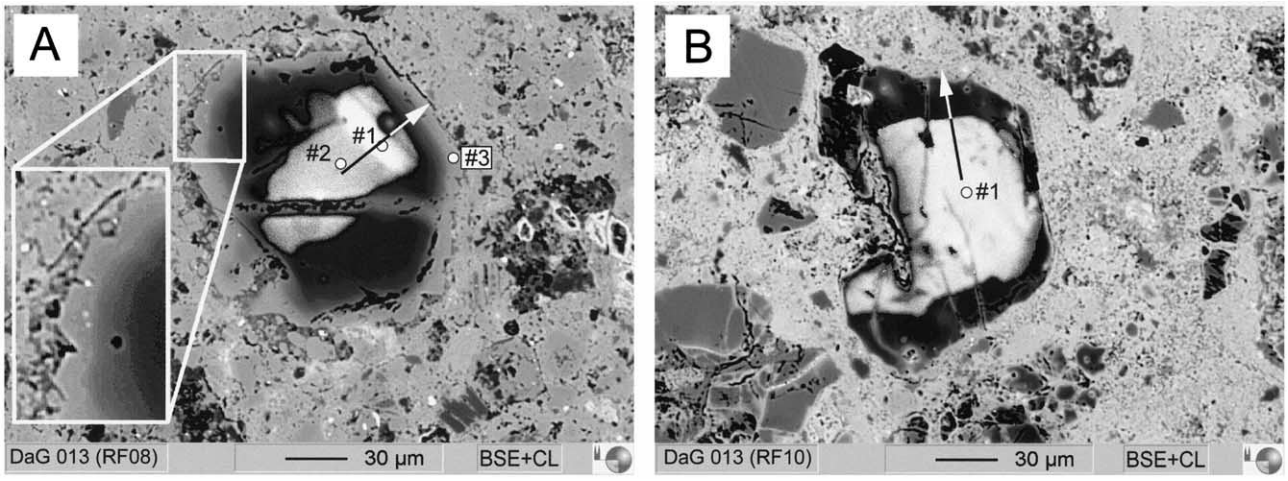

Fig. 14. Isolated refractory forsterite grains from R-chondrite Dar al Gani 013. Positions of ion probe O-isotope analyses (Fig. 16) as well as of chemical profiles (see Fig. 15) are indicated. (A) Isolated refractory forsterite DaG013/RF08 comprises of a luminescent core ($fa_{0.4}$) and is rimmed by an apparently epitaxial overgrowth of ferrous olivine ($fa_{\approx 11}$). A zone with unusual bright CL emission is enriched in Al_2O_3 (0.6 wt%). Note the well developed crystal faces bordering the fayalite rim (enlarged section). (B) Isolated refractory forsterite DaG013/RF10 with uniform bright CL emission in the core and a rim of more ferrous, nonluminous olivine.

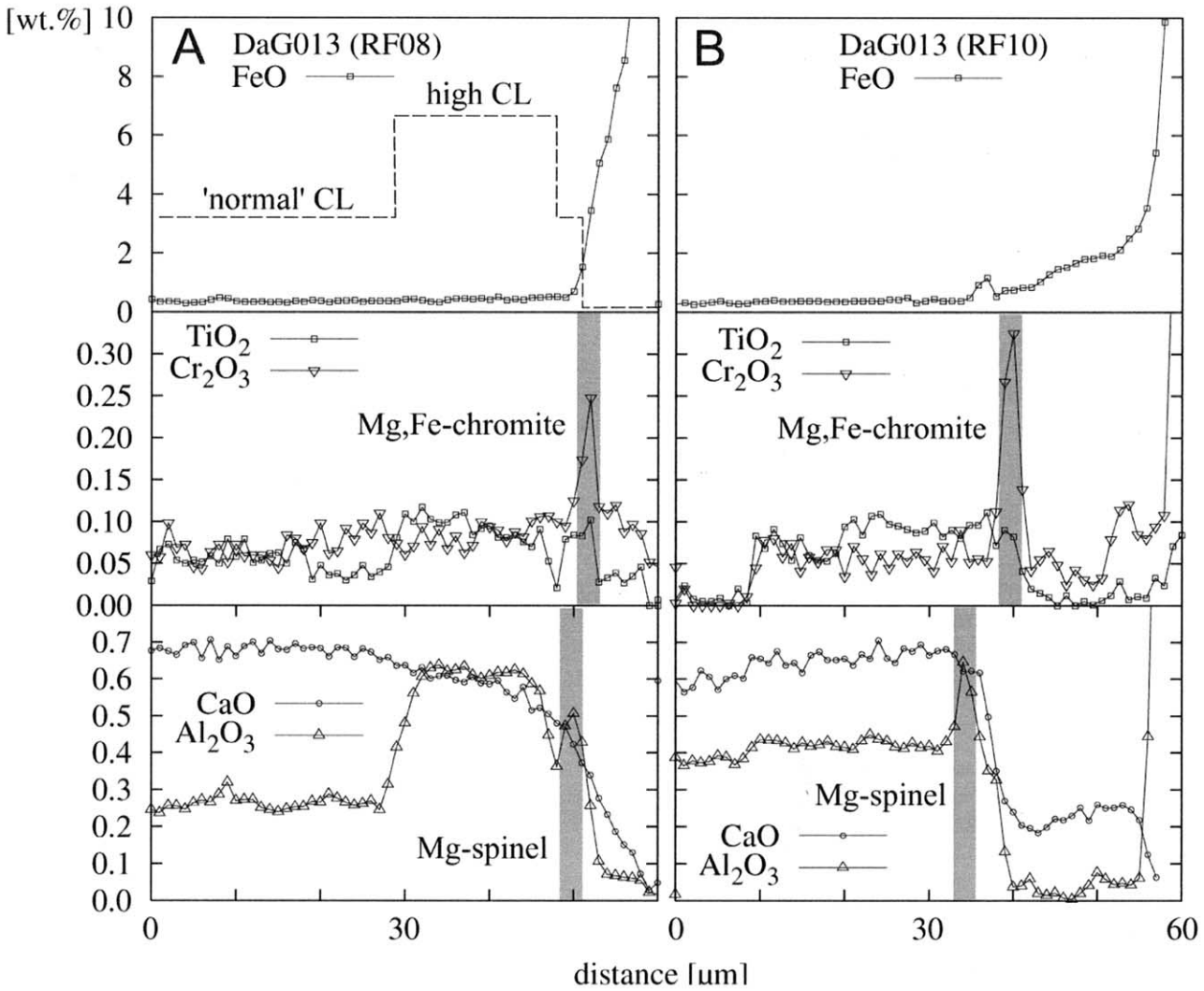

Fig. 15. EPMA chemical profiles measured across refractory forsterites DaG013/RF08 (A) and DaG013/RF10 (B) from Dar al Gani 013 (see Figs. 14A,B). The increase in Al_2O_3 and Cr_2O_3 between refractory core and fayalitic rim is due to dispersed spinel and chromite inclusions (Weinbruch et al., 1990).

sates evolves with progressive condensation of components from the gas phase. The condensation calculations indicate that melt condensates continuously change their composition due to condensation of components from the gas phase in a cooling nebula environment (Ebel and Grossman, 2000). Forsterite can grow from a melt over a temperature range of ≈160 K, before reacting with the melt to form pyroxene. According to Ebel and Grossman (2000), the CaO content of the melt gradually decreases by 30% within the temperature interval from 1782 to 1620 K. Concentrations of FeO, NiO and CoO are low in the melt, since these elements, at 1690 K would condense into of Fe-, Ni-metal and not into silicates and/or silicate liquids. As a result of the changing composition, early forsterite would have higher CaO-contents than later crystallizing forsterites. Fractional crystallization of a single forsterite grain over the whole temperature range will lead to Ca-zoning similar to what is observed in refractory forsterites (Fig. 1C). The cores would be high in CaO, whereas the rims would contain less CaO, but would be more FeO-rich. More complex zoning patterns in some refractory forsterites (e.g., Fig. 15) may reflect a more complex history of the melt from which the forsterite crystallized. The general trend of decreasing CaO with increasing FeO in all highly refractory forsterites is readily explained with the OSFC model.

Higher D/Gs than 100×solar result in higher O/H-ratios and hence in a more oxidizing nebula. In such an environment, the condensed melt will become too FeO-rich and too CaO-poor to crystallize refractory forsterites (Ebel and Grossman, 2000). D/Gs <100×solar are compatible with the extremely low FeO, MnO and NiO contents of the refractory forsterites (Palme and Fegley, 1990) but would generally lead to a decrease of the amount of melt condensates (Ebel and Grossman, 2000, their figs. 6 and 7). At D/G = 100×solar, $p^{tot} = 10^{-3}$ bar and a temperature of 1700 K, the ratio of forsterite to liquid is 3:1 with a trend of decreasing melt volume with decreasing D/G and decreasing p^{tot}. The observed fraction of refractory forster-

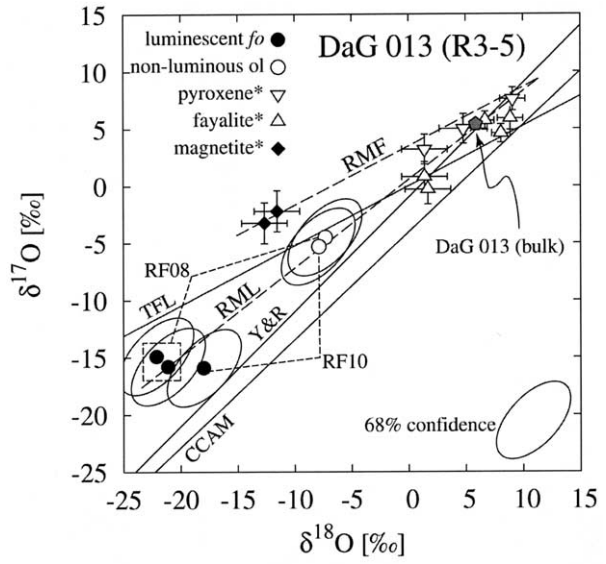

Fig. 16. Oxygen isotope ratios of refractory forsterite grains from R-chondrite Dar al Gani 013. The refractory cores (solid circles) are highly enriched in ^{16}O relative to the fayalitic rims (open circles) and the bulk composition of Dar al Gani 013. In addition, data of ferrous silicates and magnetite from R-chondrite PCA91241 (Greenwood et al., 2000) are displayed (indicated by '*'). 'RML' denotes the proposed R-chondrite mixing line and 'RMF' the R-chondrite slope-0.52 mass fractionation line at $\Delta^{17}O \approx +3‰$.

ites in bulk meteorites of only <0.4 vol% (Table 2) reflect crystallization of refractory forsterites at D/G <100×solar and/or $p^{tot} < 10^{-3}$ bar with only small amounts of melt present. Melt inclusions in refractory forsterites can be explained in this model as condensed melts (Fuchs et al., 1973; Yoneda and Grossman, 1995; Weinbruch et al., 2000) that were trapped during crystallization of forsterite.

The occurrence of refractory, Ca-rich forsterites in extremely Ca-poor, Al_2O_3- and alkali-rich mesostasis glass (Figs. 5A, 8A,B) from Dar al Gani 369 and 378 cannot be explained in terms of growth from condensed melts, which should have low alkali contents and largely unfractionated RLE abundances (Ebel and Grossman, 2000). The strong $(Ca/Al)_{meso}/(Ca/Al)_{CI}$ fractionation and the high alkali contents of the mesostasis glass of DaG369/RF02 could indicate either formation of the chondrule from a highly fractionated mineral precursor material (e.g., mixture of forsterite and Na, K-feldspar and/or nepheline) or selective removal of Ca from the chondrule. Such a process was described by Ikeda and Kimura (1996), who proposed that chondrule glasses can loose Ca during alkali-Ca metasomatism.

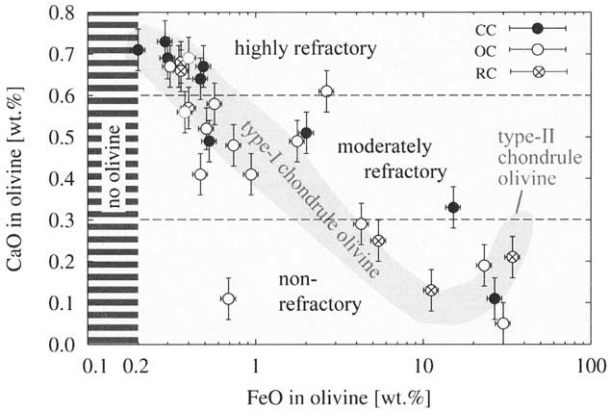

Fig. 17. Plot of CaO vs. FeO (log-scale) of olivines from CCs, OCs and RC Dar al Gani 013. The data indicate a continuum between highly refractory and nonrefractory "normal" ferrous olivine. The gray shaded area outlines the compositional variation of isolated and chondrule olivines from various types of UOCs and CCs (McSween, 1977; Leshin et al., 1997; Brearley and Jones, 1998). The error bars indicate the estimated 1σ accuracies.

The high CaO-content (0.56 wt%, Table 2) in the luminescent, moderately refractory forsterite phenocryst (Fig. 5A) in DaG369/RF02 is evidence that the chondrule initially contained ≈19 wt% CaO (Libourel, 1999), if alkalis were absent in the unaltered chondrule before alkali-Ca metasomatism. The Al_2O_3 concentration of the mesostasis glass is ≈21 wt%. Assuming that the chondrule initially had a chondritic Ca/Al ratio, the above Al_2O_3 concentration leads to a CaO content of 17 wt%. The CI Al_2O_3/TiO_2 ratio is 22.6 (Anders and Grevesse, 1989), close to the ratios in the mesostasis glass of 21.3 supporting the idea that chondrule DaG369/RF02 had initially unfractionated high RLEs and selectively lost Ca. This model, however, cannot explain the extremely high Na_2O content of the glass inclusion in the luminescent forsterite in this chondrule, which remains somewhat enigmatic. The inclusion as well as the mesostasis appear glassy under crossed nicols which points to the absence or only very limited alteration (Na-enrichment) on the parent body.

4.4. Oxygen Isotope Ratios

Refractory forsterites are excellent candidates to trace the oxygen isotope evolution of the early solar system. The pristine nature of the refractory forsterites with their very low FeO contents excludes major post crystallization alterations either in an oxidized nebula (e.g., Weinbruch et al., 1990; Bischoff, 1998; Weisberg and Prinz, 1998) or at lower temperatures on a parent body (Krot et al., 1995, 1997, 1998; Young, 2001).

Figure 19 shows a compilation of SIMS analyses of olivine grains from UOCs, CCs and RC Dar al Gani 013. Data from UOCs are from this study (LL3, L3, H3), Saxton et al. (1998, Julesburg, L3.6) and Sears et al. (1998, Semarkona), LL3.0. Data from CCs are from this study (Murchison, CM; Renazzo, CR; Allende, CV), Leshin et al. (1997, Orgueil, CI) and Jones et al. (2000a, ALHA77307, CO). Further data from Allende are from Hervig and Steele (1992), Weinbruch et al. (1993), Saxton et al. (1998), Maruyama et al. (1999) and Klerner et al. (unpublished data). Figure 19 includes data from refractory forsterites as well as from more ferroan olivines. No apparent difference is indicated between olivines from ordinary and carbonaceous chondrites. The results of this study plot in the same range as results from previous studies.

Not only olivines from OCs, but also those from CCs plot on average closer to the Y&R-line than to the CCAM line (Fig. 19; Jones et al., 2000a, their fig. 6; Leshin et al., 1997). This may indicate that the Y&R line of slope 1.0 is the relevant primordial mixing line (a) for UOCs and (b) for CCs. More data are necessary to clarify whether refractory forsterites from R-chon-

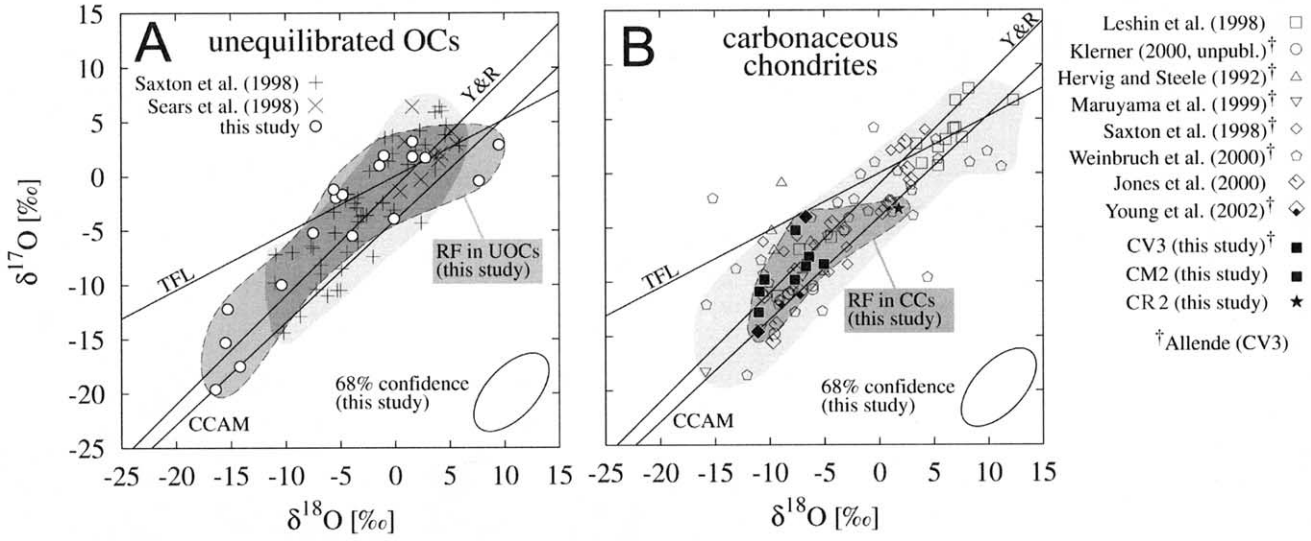

Fig. 18. Sketch illustrating the formation model for refractory forsterites by crystallization within early melt condensates.

drites plot on a different line in the 3-O-isotope diagram or, together with forsterites from OCs and CCs, close to the Y&R line.

Highly refractory forsterites (i.e., >0.6 wt% CaO) are without exception enriched in ^{16}O with $\Delta^{17}O$ between -4 and $-10‰$ (Fig. 20), whereas moderately and nonrefractory olivines cover a range between $\Delta^{17}O = -5$ and $+2‰$ (Fig. 20). There is no difference in chemical and isotopic composition of highly refractory forsterites from UOCs, CCs and RC Dar al Gani 013 (Fig. 20). This indicates that this subpopulation of forsterites formed by the same process, possibly from a single reservoir that was decoupled from the oxidation state and O-isotope composition of the host meteorite. In this regard, refractory forsterites are similar to CAIs, that occur in UOCs (McKeegan et al., 1998), CCs (Brearley and Jones, 1998) and RCs (Bischoff and Srinivasan, 2003). Leshin et al. (1997) have demonstrated that the enrichment in ^{16}O correlates with the FeO-content of isolated olivine grains from Orgueil (CI).

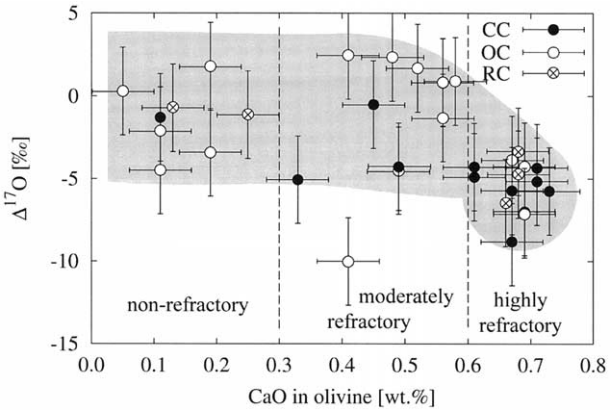

Fig. 19. Plot of $\delta^{17}O$ vs. $\delta^{18}O$ of in situ analyses of olivine from (A) UOCs and (B) CCs.

Hence, ^{16}O-rich forsterites have high RLE and low FeO contents, respectively.

Oxygen isotope ratios were measured on two olivines and their spinel inclusions (Figs. 3A, 11B, Table 3). Similar $\Delta^{17}O$ values of nonluminous (fo_{98}) olivine host and spinel inclusion in Mur/RF07 (Figs. 10E, 11B) indicate cogenetic formation in a closed system. The difference in $\delta^{18}O$ is opposite to what is expected in case of mass-dependent fractionation between olivine and spinel (Zheng, 1991, 1993) and may be due to the analytical uncertainty. The error ellipses of the estimated accuracy of 95% confidence of olivine and spinel overlap. Forsterite Mur/RF07 with its spinel inclusion could very well have crystallized in a type-I chondrule. This conclusion is supported by the $\Delta^{17}O$ of olivine and spinel which is similar to bulk CC chondrules.

The spinel inclusions in the large luminescent, highly refractory forsterite Cha/C1 are significantly enriched in ^{16}O relative to the forsterite host. Russell et al. (2000) explained the disequilibrium O-isotope ratios between individual minerals of high-Al chondrules by melting of an initially ^{16}O-rich chondrule precursor material in an ^{16}O depleted nebular environment. Assuming a cogenetic origin of spinel inclusions and forsteritic host, the disequilibrium between spinel and forsterite points to a change in the ^{16}O-content of the liquid during or after crystallization of the spinel ($\Delta^{17}O \approx -10‰$), before olivine crystallization ($\Delta^{17}O \approx -6‰$). Although we cannot rule out the validity of the model of Russell et al. (2000), we suggest a slightly modified version for formation of the forsterite-spinel disequilibrium associations in Cha/C1, which is in agreement to our OSFC model. We suggest that the spinel crystallized in an ^{16}O-rich and highly refractory melt condensate at temperatures slightly above the forsterite appearance temperature of around 1790 K (Ebel and Grossman, 2000). The change of melt composition due to condensation of common lithophile elements (Si, Mg) was accompanied by a gradual

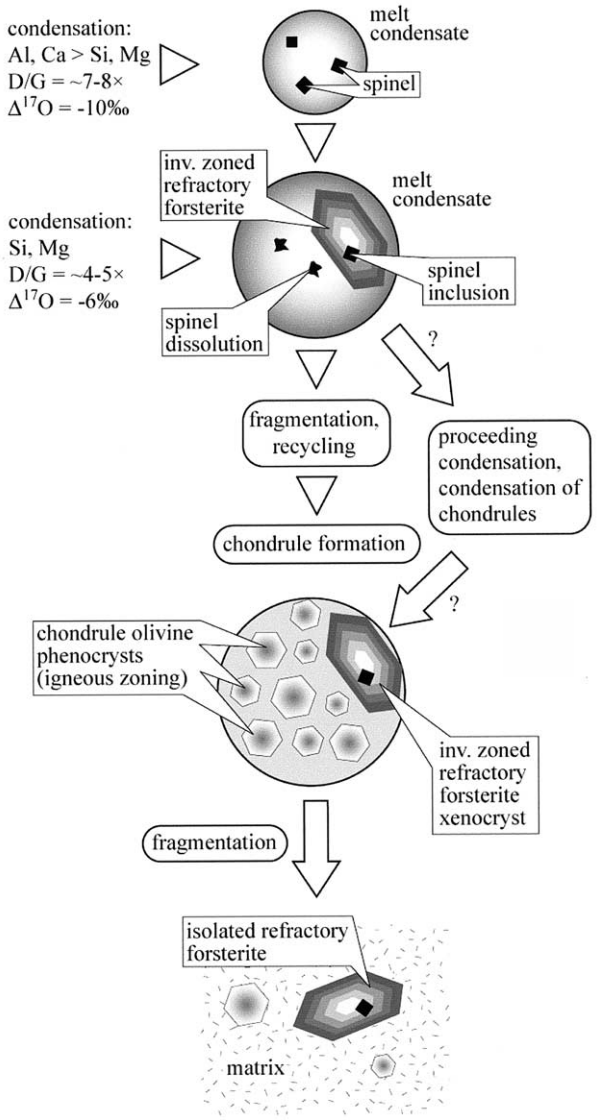

Fig. 20. Plot of $\Delta^{17}O$ vs. CaO content of olivine grains. The highly refractory forsterites with >0.6 wt% CaO are exclusively enriched in ^{16}O. The error bars indicate the estimated 1σ accuracies.

change in O-isotope composition from $\Delta^{17}O \approx -10‰$ to $\approx -6‰$.

4.5. O-Isotopic Evolution of the Solar Nebula

The large oxygen isotope heterogeneity in chondritic meteorites can be explained by mixing of ^{16}O-rich silicate and oxide dust with ^{16}O-poor gas (CO, H_2O, Clayton, 1993). Scott and Krot (2001) and Krot et al. (2002) proposed that the ^{16}O-rich CAIs must have condensed from evaporated dust in an environment with high initial D/G and hence low $\Delta^{17}O$. Less refractory material formed by condensation from a gas in an environment with once lower initial D/G.

According to the model of Scott and Krot (2001) the oxygen isotope composition of the highly refractory forsterites ($\delta^{17,18}O \approx -15‰$) can be achieved by evaporation of ^{16}O-rich dust in a system with D/G = 4–5×solar (Scott and Krot, 2001, their fig. 3). Based on the low FeO-contents of refractory forsterites, we have proposed that the melts parental to refractory forsterites condensed in an environment with D/G <100×solar. Hence, 4–5×solar is well within the predicted range. We suggest that ^{16}O-rich spinel crystallized from condensed melts before forsterite. At the time of spinel crystallization, the nebula had an oxygen isotope composition near $\delta^{17,18}O \approx -20‰$, which can be achieved at D/G = 7–8×solar (Scott and Krot, 2001, their fig. 3). The change in oxygen isotope composition of the ambient gas could be achieved by successive addition of low-^{16}O gas (CO, H_2O) and/or ice to the high-^{16}O evaporates.

One problem with this model is that melt condensates are not stable at such low D/G ratios (assuming $p^{tot} = 10^{-3}$ bar, Ebel and Grossman, 2000). Possibly $\Delta^{17}O$ of the melt condensates and hence of spinel and forsterite were initially lower ($\Delta^{17}O \approx -15‰$, D/G ≈ 20×solar), but exchange with the increasingly ^{16}O-poor nebula shifted $\Delta^{17}O$ towards the values observed in spinel and highly refractory forsterites (Russell et al., 2000).

5. CONCLUSIONS

Similarities in abundance, chemical and O-isotope composition indicate that highly refractory forsterites from the different types of chondrites formed from in the same process, possibly from a single reservoir. We propose that highly refractory, ^{16}O-rich forsterites formed by open system, fractional crystallization within droplets of RLE-rich condensed melt (Fig. 17).

Clayton and coworkers (e.g., 1977, 1983, 1999) have shown a correlation between chemical composition and enrichment of ^{16}O in extraterrestrial samples. Until the apparently unique discovery of an extreme ^{16}O-rich chondrule from CH chondrite Acfer 214 by Kobayashi et al. (2003), high-T, RLE-rich condensates (CAIs) showed the highest enrichments in ^{16}O of solar system materials ($\delta^{17,18}O \approx -50‰$). Less refractory components have only little (chondrules) or no excess ^{16}O (matrix) relative to terrestrial material. The oxygen isotope ratio is furthermore correlated with the degree of oxidation. Highly reduced CAIs have low $\Delta^{17}O$, whereas matrix magnetite from UOCs shows the highest $\Delta^{17}O$ of chondrite components (Choi et al., 1998).

A trend of decreasing ^{16}O with decreasing 'degree of refractoriness' (i.e., decreasing RLE contents) is also observed within bulk chondrules of the same meteorite (Rubin and Wasson, 1987; Rubin et al., 1990). Young et al. (2002) report high-precision O- and Mg-isotope data of chondrules from Allende. The most FeO-poor, and presumably most RLE-rich forsterites exhibit the highest enrichment in ^{16}O ($\Delta^{17}O = -7.2‰$, chondrule 'C8') whereas the more ferroan olivines in barred olivine chondrule are less enriched in ^{16}O ($\Delta^{17}O = -2.8‰$, chondrule 'C6'). A similar relationship is reported by Leshin et al. (1997) from isolated olivine grains from Orgueil (CI). Our data from olivines follow a similar trend: highly refractory forsterites (>0.6 wt% CaO) are, on an average, richer in ^{16}O than moderately or nonrefractory forsterites (Fig. 20).

Refractory inclusions (CAIs) may be generally *older* than less refractory, more Si- and Mg-rich components, like chondrules (Amelin et al., 2002). Using the ^{26}Al-$^{26}Mg^*$ chronometer, Tachibana et al. (2001) have shown that chondrules depleted in moderately volatile elements (i.e., low ([Na, Mn,

Cr]/Mg)-ratios) may be generally older than those with higher ([Na, Mn, Cr]/Mg)-ratios, provided ^{26}Al was initially homogenous. This trend is also reflected in the mineralogy of chondrules; olivine-rich chondrules may be generally older than pyroxene-rich chondrules (Tachibana et al., 2001; Mostefaoui et al., 2002). Again, more refractory components are apparently older then less refractory components.

Since highly refractory forsterites (and their proposed host melts) are intermediate in O-isotope as well as in chemical composition between CAIs and chondrules, we suggest the formation of refractory forsterites occurred in a time gap between formation of CV CAIs (4567.2 ± 0.6 Ma, Amelin et al., 2002) and formation of CR chondrules ≈2.5 Ma later (4564.7 ± 0.6 Ma, Amelin et al., 2002). This hypothesis is consistent with the occurrence of highly refractory forsterites as relicts within chondrules, which is indicative of formation of most of the refractory forsterites before chondrule formation.

Acknowledgments—A. Bischoff (Münster), J. Zipfel (Mainz) and R. H. Jones (Albuquerque) are thanked for loaning polished thin sections of unequilibrated ordinary and R-chondrites. D. Ebel, E. Young and an anonymous reviewer are thanked for their thorough and constructive reviews. This work was financially supported by the German Science Foundation (DFG, grant PA 346/24–1).

Associate editor: S. S. Russell

REFERENCES

Agee C. B. and Walker D. (1990) Aluminum partitioning between olivine and ultrabasic silicate liquid to 6 GPa. *Contrib. Mineral. Petrol.* **105,** 243–254.

Amelin Y., Krot A. N., Hutcheon I. D., and Ulyanov A. A. (2002) Lead isotopic ages of chondrules and calcium-aluminum-rich inclusions. *Science* **297,** 1678–1683.

Anders E. and Grevesse N. (1989) Abundances of the elements: Meteoric and solar. *Geochim. Cosmochim. Acta* **53,** 197–214.

Berman R. G. (1983) A thermodynamic model for multicomponent melts, with application to the system CaO–MgO–Al_2O_3–SiO_2. Ph.D. thesis. University of British Columbia.

Bischoff A. (1998) Aqueous alteration of carbonaceous chondrites: Evidence for preaccretionary alteration—A review. *Meteor. Planet. Sci.* **33,** 1113–1122.

Bischoff A. (2000) Mineralogical characterization of primitive, type-3 lithologies in Rumurutiiti chondrites. *Meteor. Planet. Sci.* **35,** 699–706.

Bischoff A. and Srinivasan G. (2003) Mg-26 excess in hibonites of the Rumuruti chondrite Hughes 030. *Meteor. Planet. Sci.* **38,** 5–12.

Blum J. and Munch M. (1993) Experimental investigations of aggregate-aggregate collisions in the early solar nebula. *Icarus* **106,** 151–167.

Brearley A. J. and Jones R. H. (1998) Chondritic meteorites. *Rev. Mineral.* **36,** 3-1-3-398.

Choi B.-K., McKeegan K. D., Krot A. N., and Wasson J. T. (1998) Extreme oxygen-isotope composition in magnetite from unequilibrated ordinary chondrites. *Nature* **392,** 577–579.

Clayton R. N. (1993) Oxygen isotopes in meteorites. *Annu. Rev. Earth Sci.* **21,** 115–149.

Clayton R. N., Onuma N., Grossman L., and Mayeda T. K. (1977) Distribution of the pre-solar component in Allende and other carbonaceous chondrites. *Earth Planet. Sci. Lett.* **34,** 209–224.

Clayton R. N., Onuma N., Ikeda Y., and Mayeda T. K. (1983) Oxygen isotope composition of chondrules in Allende and ordinary chondrites. In *Chondrules and Their Origins* (ed. E. A. King), pp. 37–43. Lunar and Planetary Science Institute.

Clayton R. N., Mayeda T. K., Goswami J. N., and Olsen E. J. (1991) Oxygen isotope studies of ordinary chondrites. *Geochim. Cosmochim. Acta* **55,** 2317–2337.

Clayton R. N. and Mayeda T. K. (1999) Oxygen isotopes of carbonaceous chondrites. *Geochim. Cosmochim. Acta* **63,** 2089–2104.

Desnoyers C. (1980) The Niger (I) carbonaceous chondrite and implications for the origin of aggregates and isolated olivine grains in C2 chondrites. *Earth Planet. Sci. Lett.* **47,** 223–234.

Ebel D. (2000) Variations on solar condensation: Sources of interstellar dust nuclei. *J. Geophys. Res. Space Phys.* **105,** 10363–10370.

Ebel D. and Grossman L. (2000) Condensation in dust-enriched systems. *Geochim Cosmochim Acta* **64,** 339–366.

Fuchs L. H., Olsen E., and Jensen K. J. (1973) Mineralogy, mineral-chemistry and composition of the Murchison (C2) meteorite. *Smith. Contrib. Earth Sci.* **10,** 1–39.

Ghiorso M. S. and Sack R. O. (1995) Chemical mass transfer in magmatic processes IV. A revised and internally consistent thermodynamic model for the interpolation and extrapolation of liquid–solid equilibria in magmatic systems at elevated temperatures and pressures. *Contrib. Mineral. Petrol.* **119,** 197–212.

Gooding J. L., Mayeda T. K., Clayton R. N., and Fukuoka T. (1983) Oxygen isotope heterogeneities, their petrological correlations, and implications for melt origins of chondrules in unequilibrated chondrites. *Earth Planet. Sci. Lett.* **63,** 209–224.

Greenwood J. P., Rubin A. E., and Wasson J. T. (2000) Oxygen isotopes in R-chondrite magnetite and olivine: Link between R chondrites and ordinary chondrites. *Geochim. Cosmochim. Acta* **64,** 3897–3911.

Grossman L. (1972) Condensation in the primitive solar nebula. *Geochim. Cosmochim. Acta* **36,** 597–620.

Grossman L. and Olsen E. (1974) Origin of the high-temperature fraction of C2 chondrites. *Geochim. Cosmochim. Acta* **38,** 173–187.

Grossman J. N. and Wasson J. T. (1983) Refractory precursor components of Semarkona chondrules and the fractionation of refractory elements among chondrules. *Geochim. Cosmochim. Acta* **47,** 759–771.

Hervig R. L. and Steele I. M. (1992) Oxygen isotope analysis of Allende olivine by ion probe and implications for chondrule origin. *Lunar Planet. Sci.* **33,** 525–526.

Ikeda Y. and Kimura M. (1996) Anhydrous alteration of Allende chondrules in the solar nebula III: Alkali-zoned chondrules and heating experiments for anhydrous alteration. *Proc. NIPR Symp. Antarct. Meteorites* **9,** 51–68.

Jäckel A., Bischoff A., Clayton R. N., and Mayeda T. K. (1996) Dar al Gani 013—A new Rumuruti-like chondrite (R3-6) with highly unequilibrated (type 3) fragments. *Lunar Planet. Sci.* **27,** 595–596.

Jones R. H. (1992) On the relationship between isolated and chondrule olivine grains in carbonaceous chondrite ALHA77307. *Geochim. Cosmochim. Acta* **56,** 467–482.

Jones R. H. (1996) Relict grains in chondrules: Evidence for chondrule recycling. In *Chondrules and the ProtoPlanetary Disk* (eds. R. H. Hewins, R. H. Jones, and E. R. D. Scott), pp. 163–172. Cambridge University Press.

Jones R. H. and Scott E. R. D. (1989) Petrology and thermal history of type-IA chondrules in the Semarkona (LL3.0) chondrite. *Lunar Planet. Sci.* **19,** 523–536.

Jones R. H., Saxton J. M., Lyon I. C., and Turner G. (2000a) Oxygen isotopes in chondrule olivine and isolated olivine grains from the CO3 chondrite Allan Hills A77307. *Meteor. Planet. Sci.* **35,** 849–857.

Jones R. H., Durakiewicz T., Sharp Z. D., and Schilk A. J. (2000b) Oxygen isotope ratios of bulk chondrules from the Mokoia CV3 chondrite (abstract). *Meteor. Planet. Sci.* **35,** A84.

Kennedy A. K., Lofgren G. E., and Wasserburg G. J. (1993) An experimental study of trace element partitioning between olivine, orthopyroxene and melt in chondrules: Equilibrium values and kinetic effects. *Earth Planet. Sci. Lett.* **115,** 177–195.

Klerner S. (2001) Materie im frühen Sonnensystem: Die Entstehung von Matrix, Chondren und refraktärem Forsterit. Ph.D. thesis. Universität zu Köln, 119 p.

Klerner S., Jones R. H., Palme H., and Shearer C. K. (2000) Trace elements and cathodoluminescence in refractory forsterite from Allende and Kaba. *Lunar Planet. Sci.* **31,** 1689.

Kobayashi S., Imai H., and Yurimoto H. (2003) An extreme ^{16}O-rich chondrule from ACFER 214 CH chondrite. *Lun. Planet. Sci.* **34,** 1539.

Krot A. N., Scott E. R. D., and Zolensky M. E. (1995) Mineralogical and chemical midification of components in CV3 chondrites: Nebular or asteroidal processing? *Meteoritics* **30,** 748–776.

Krot A. N., Scott E. R. D., and Zolensky M. E. (1997) Origin of fayalitic olivine rims and lath-shaped matrix olivine in CV3 chondrite Allende and its dark inclusions. *Meteor. Planet. Sci.* **32,** 31–49.

Krot A. N., Petaev M. I., Scott E. R. D., Choi B.-G., Zolensky M. E., and Keil K. (1998) Progressive alteration in CV3 chondrites: More evidence for asteroidal alteration. *Meteor. Planet. Sci.* **33,** 1065–1085.

Krot A. N., McKeegan K. D., Leshin L. A., MacPherson G. J., and Scott E. R. D. (2002) Existence of an ^{16}O-rich gaseous reservoir in the solar nebula. *Science* **295,** 1051–1054.

Larimer J. W. and Anders E. (1967) Chemical fractionation in meteorites. 2. Abundance patterns and their interpretation. *Geochim. Cosmochim. Acta* **31,** 1239–1270.

Leshin L. A., Rubin A. E., and McKeegan K. D. (1997) The oxygen isotopic composition of olivine and pyroxene from C1 chondrites. *Geochim. Cosmochim. Acta* **61,** 835–845.

Leshin L. A., McKeegan K. D., Engrand C., Zanda B., Bourot-Denise M., and Hewins R. H. (1998) Oxygen isotopic studies of isolated and chondrule olivine from Renazzo and Allende (abstract). *Meteor. Planet. Sci.* **33,** A93–A94.

Leshin L. A., McKeegan K. D., and Bendix G. K. (2000) Oxygen isotope geochemistry of olivine from carbonaceous chondrites. *Lunar Planet. Sci.* **31,** 1918.

Libourel G. (1999) Systematics of calcium partitioning between olivine and silicate melt: Implications for melt structure and calcium content of magmatic systems. *Contrib. Mineral. Petrol.* **136,** 63–80.

Maruyama S., Yurimoto H., and Sueno S. (1999) Oxygen isotope evidence regarding the formation of spinel-bearing chondrules. *Earth Planet. Sci. Lett.* **169,** 165–171.

McKeegan K. D., Leshin L. A., Russell S. S., and MacPherson G. J. (1998) Oxygen isotopic abundances in calcium-aluminum-rich inclusions from ordinary chondrites: Implications for nebular heterogeneity. *Science* **280,** 414–418.

McSween H. Y. Jr. (1977) On the nature and origin of isolated olivine grains in carbonaceous chondrites. *Geochim. Cosmochim. Acta* **41,** 411–418.

Mostefaoui S., Kita N. T., Togashi S., Tachibana S., Nagahara H., and Morishita Y. (2002) The relative formation ages of ferromagnesian chondrules inferred from their initial aluminum-26/aluminum-27 ratios. *Meteor. Planet. Sci. Lett.* **37,** 421–438.

Olsen E. and Grossman L. (1978) On the origin of isolated olivine grains in Type 3 carbonaceous chondrites. *Earth Planet. Sci. Lett.* **41,** 111–127.

Pack A., Sauerborn M., Klerner S., Palme H., Neumann A. and Seboldt W. (2002a) Dynamic crystallization experiments using conventional and solar furnace techniques—Implications for the formation of refractory forsterite in chondrites. *Eur. Geophys. Union Gen. Ass.* **27,** EGS02-A-01829-4.

Pack A., Yurimoto H., and Palme H. (2002b) Oxygen isotopic composition of refractory forsterite in R-chondrite Dar al Gani 013, unequilibrated ordinary, and carbonaceous chondrites. *Lunar Planet. Sci.* **33,** 1666.

Pack A. and Palme H. (2003) Partitioning of Ca and Al between forsterite and silicate melt in dynamic systems with implications for the origin of Ca, Al-rich forsterites in primitive meteorites. *Meteor. Planet. Sci.* **38,** 1263–1281.

Pack A., Shelley M., O'Neill H. St. C. and Palme H. (2003) An in-situ trace element study of refractory forsterites from different types of unequilibrated chondrites. *Lunar Planet. Sci.* **34,** 1600.

Palme H. and Fegley B. Jr. (1990) High-temperature condensation of iron-rich olivine in the solar nebula. *Earth Planet. Sci. Lett.* **101,** 180–195.

Palme H., Spettel B., Kurat G., and Zinner E. (1992) Origin of Allende chondrules. *Lunary Planet. Sci.* **23,** 1021–1022.

Palme H. and Beer H. (1993) Abundances of the elements in the solar system. In *Instruments; Methods; Solar System* (ed. H. H. Voigt), pp. 196–221. Landolt-Börnstein, Group 6: Astronomy and Astrophysics, Vol. 3a. Springer-Verlag.

Peck J. A. and Wood J. A. (1987) The origin of ferrous zoning in Allende chondrule olivines. *Geochim. Cosmochim. Acta* **51,** 1503–1510.

Reid A. M., Bass M. N., Fujita H., Kerridge J. F., and Frederiksson K. (1970) Olivine and pxyroxene in the Orgueil meteorite. *Geochim. Cosmochim. Acta* **34,** 1253–1255.

Richardson S. M. and McSween H. Y. Jr. (1978) Textural evidence bearing on the origin of isolated olivine crystals in C2 carbonaceous chondrites. *Earth Planet. Sci. Lett.* **37,** 485–491.

Roedder E. (1981) Significance of Ca-Al-rich silicate melt inclusions in olivine crystals from the Murchison type II carbonaceous chondrite. *Bull. Minéral.* **104,** 339–353.

Rubin A. E. and Wasson J. T. (1987) Chondrules, matrix and coarse-grained chondrule rims in the Allende meteorite: Origin, interrelationship and possible precursor components. *Geochim. Cosmochim. Acta* **51,** 1923–1937.

Rubin A. E., Wasson J. T., Clayton R. N., and Mayeda T. K. (1990) Oxygen isotopes in chondrules and coarse-grained chondrule rims from the Allende meteorite. *Earth Planet. Sci. Lett.* **96,** 247–255.

Russell S. S., MacPherson G. J., Leshin L. A., and McKeegan K. D. (2000) ^{16}O enrichments in aluminum-rich chondrules from ordinary chondrites. *Earth Planet. Sci. Lett.* **184,** 57–74.

Ruzicka A., Hiyagon H., Prinz M., and Taylor L. A. (2000) Forsteritic olivine grains in unequilibrated ordinary chondrites: Additional evidence for a link between ordinary and carbonaceous chondrites. *Lunar Planet. Sci.* **31,** 1313.

Saxton J. M., Lyon I. C., and Turner G. (1998) Oxygen isotopes in forsterite grains from Julesburg and Allende: Oxygen-16-rich material in an ordinary chondrite. *Meteor. Planet. Sci.* **33,** 1017–1027.

Schulze H., Bischoff A., Palme H., Spettel B., Dreibus G., and Otto J. (1994) Mineralogy and chemistry of Rumuruti: The first meteorite fall of the new R chondrite group. *Meteoritics* **29,** 275–286.

Scott E. R. D. and Krot A. N. (2001) Oxygen isotope composition and origins of calcium-aluminum-rich inclusions and chondrules. *Meteor. Planet. Sci. Lett.* **36,** 1307–1319.

Schneiderhöhn H. and Ramdohr P. (1934) *Lehrbuch der Erzmikroskopie*. Verlag von Gebrüder Bornträger.

Sears D. W. G., Lyon I., Saxton J., and Turner G. (1998) The oxygen isotope properties of olivines in the Semarkona ordinary chondrite. *Meteor. Planet. Sci.* **33,** 1029–1032.

Steele I. M. (1985) Cathodoluminescence zoning and minor elements in forsterites from Murchison (CM2) and Allende (CV3) carbonaceous chondrites. *Nature* **313,** 294–297.

Steele I. M. (1986a) Cathodoluminescence and minor elements in forsterites from extraterrestial samples. *Am. Mineral.* **71,** 966–970.

Steele I. M. (1986b) Compositions and textures of relict forsterite in carbonaceous and unequilibrated ordinary chondrites. *Geochim. Cosmochim. Acta* **50,** 1379–1395.

Steele I. M. (1989) Compositions of isolated forsterites in Ornans (CO3). *Geochim. Cosmochim. Acta* **53,** 2069–2079.

Steele I. M. (1995) Oscillatory zoning in meteorite forsterite. *Am. Mineral.* **80,** 823–832.

Tachibana S., Kita N. T., Nagahara H., and Mostefaoui S. (2001) Correlation between relative ages and bulk compositions of ferromagnesian chondrules from highly unequilibrated chondrules (abstract). *Meteor. Planet. Sci. Lett.* **36,** A202.

Weinbruch S., Palme H., Müller G., and El Goresy A. (1990) FeO-rich rims and veins in Allende forsterite: Evidence for high temperature condensation at oxidizing conditions. *Meteoritics* **25,** 115–125.

Weinbruch S., Zinner E., El Goresy A., Steele I. M., and Palme H. (1993) Oxygen isotopic composition of individual olivine grains from the Allende meteorite. *Geochim. Cosmochim. Acta* **57,** 2649–2661.

Weinbruch S., Palme H., and Spettel B. (2000) Refractory forsterite in primitive meteorites: Condensates from the solar nebula? *Meteor. Planet. Sci.* **35,** 161–171.

Weisberg M. K., Prinz M., Kojima H., Yanaki K., Clayton R. N., and Mayeda T. K. (1991) The Carlisle Lakes-type chondrites–A new grouplet with high Δ^{17}O and evidence for nebular oxidation. *Geochim. Cosmochim. Acta* **55,** 2657–2669.

Weisberg M. K., Prinz M., Clayton R. N., and Mayeda T. K. (1993) The CR (Renazzo-type) carbonaceous chondrite group and its implications. *Geochim. Cosmochim. Acta* **57,** 1567–1586.

Weisberg M. K. and Prinz M. (1998) Fayalitic olivine in CV3 chondrite matrix and dark inclusions: A nebular origin. *Meteor. Planet Sci.* **33,** 1087–1099.

Yoneda S. and Grossman L. (1995) Condensation of CaO-MgO-Al_2O_3-SiO_2 liquids from cosmic gases. *Geochim. Cosmochim. Acta* **59,** 3413–3444.

Young E. D. and Russell S. S. (1998) Oxygen reservoirs in the early solar nebula inferred from an Allende CAI. *Science* **282,** 425−455.

Young E. D. (2001) The hydrology of carbonaceous chondrite parent bodies and the evolution of planet progenitors. *Phil. Trans. R. Soc. Lond. A* **359,** 2095–2110.

Young E. D., Ash R. D., Galy A., and Belshaw N. S. (2002) Mg isotope heterogeneity in the Allende meteorite measured by UV laser ablation-MC-ICPMS and comparisons with O isotopes. *Geochim. Cosmochim Acta* **66,** 683−698.

Zheng Y. F. (1991) Calculation of oxygen isotope fractionation in metal oxides. *Geochim. Cosmochim. Acta* **55,** 2299–2307.

Zheng Y. F. (1993) Calculation of oxygen isotope fractionation in anhydrous silicate minerals. *Geochim. Cosmochim. Acta* **57,** 1079–1091.